



Meson-exchange currents in intermediate energy electron scattering

The semi-relativistic shell model

José Enrique Amaro

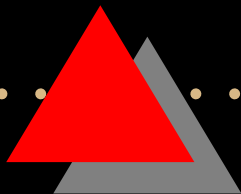
Departamento de
**FÍSICA ATÓMICA,
MOLECULAR Y NUCLEAR**





Colaboration

- M.B. Barbaro (Torino)
- J.A. Caballero (Sevilla)
- T.W. Donnelly (MIT)
- C. Maieron (Grenoble)
- J.M. Udias (UC Madrid)



Overview

1. Lepton scattering

- (e, e')
- (ν_l, l^-)

2. Scaling

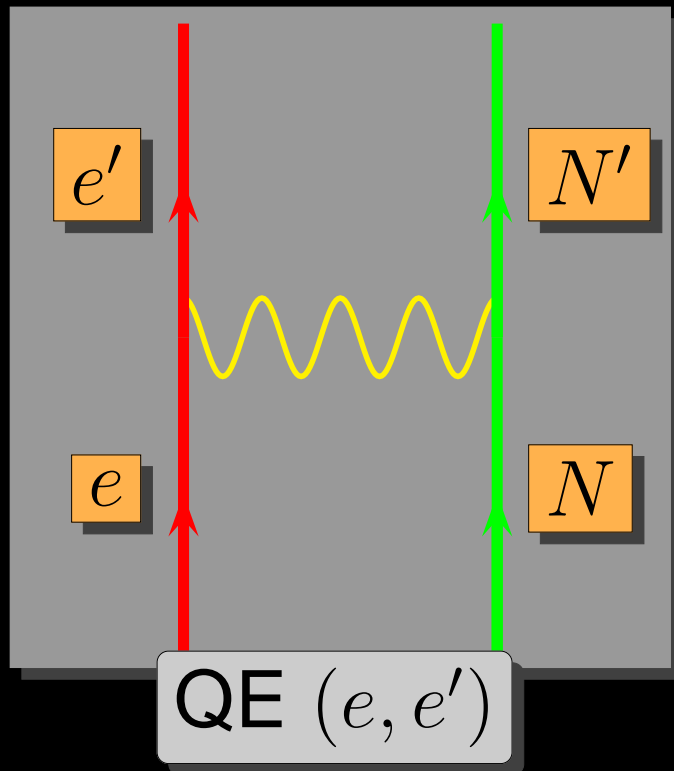
3. The Semi-Relativistic (SR) shell model

- The continuum shell model
- Final State Interaction (FSI):
DEB+Darwin potential
- Test of the SR approach
- Scaling of (e, e') response functions
- CC neutrino reactions

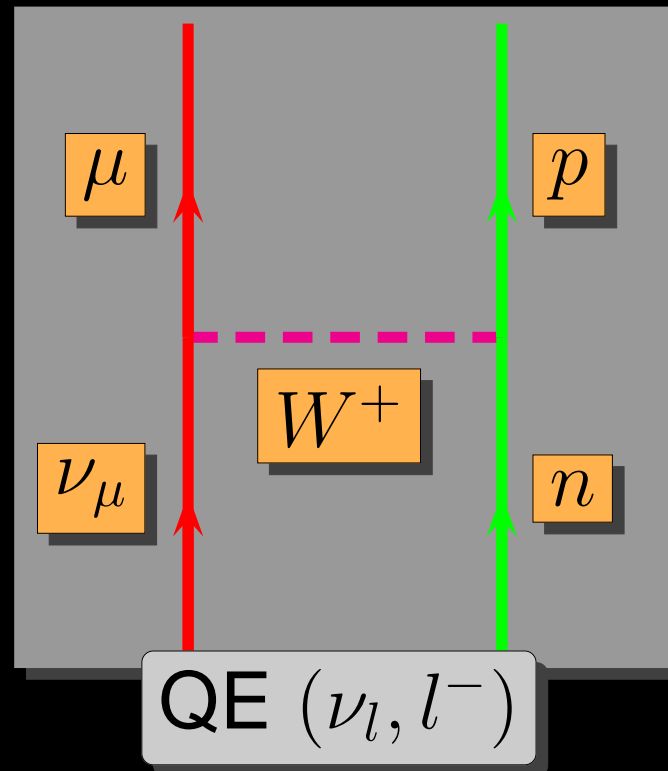
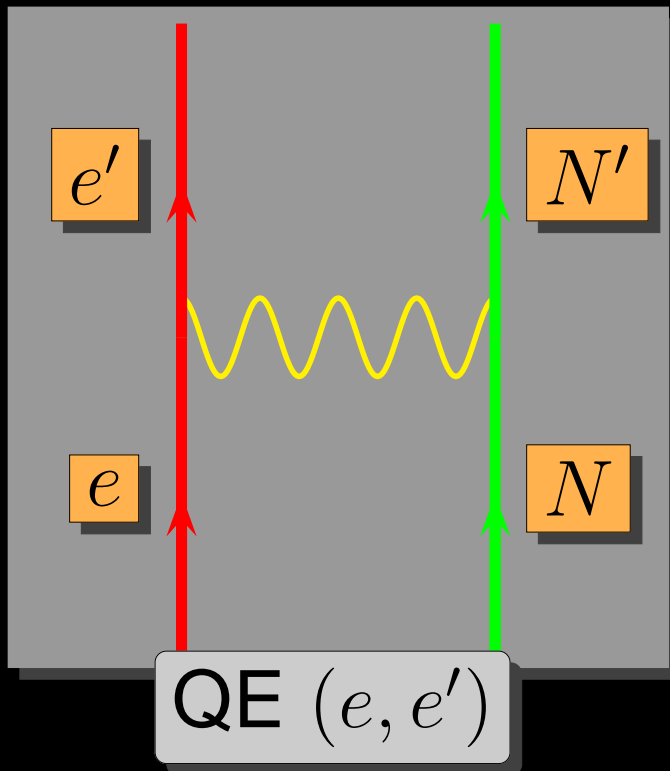
4. Meson-exchange currents (MEC)



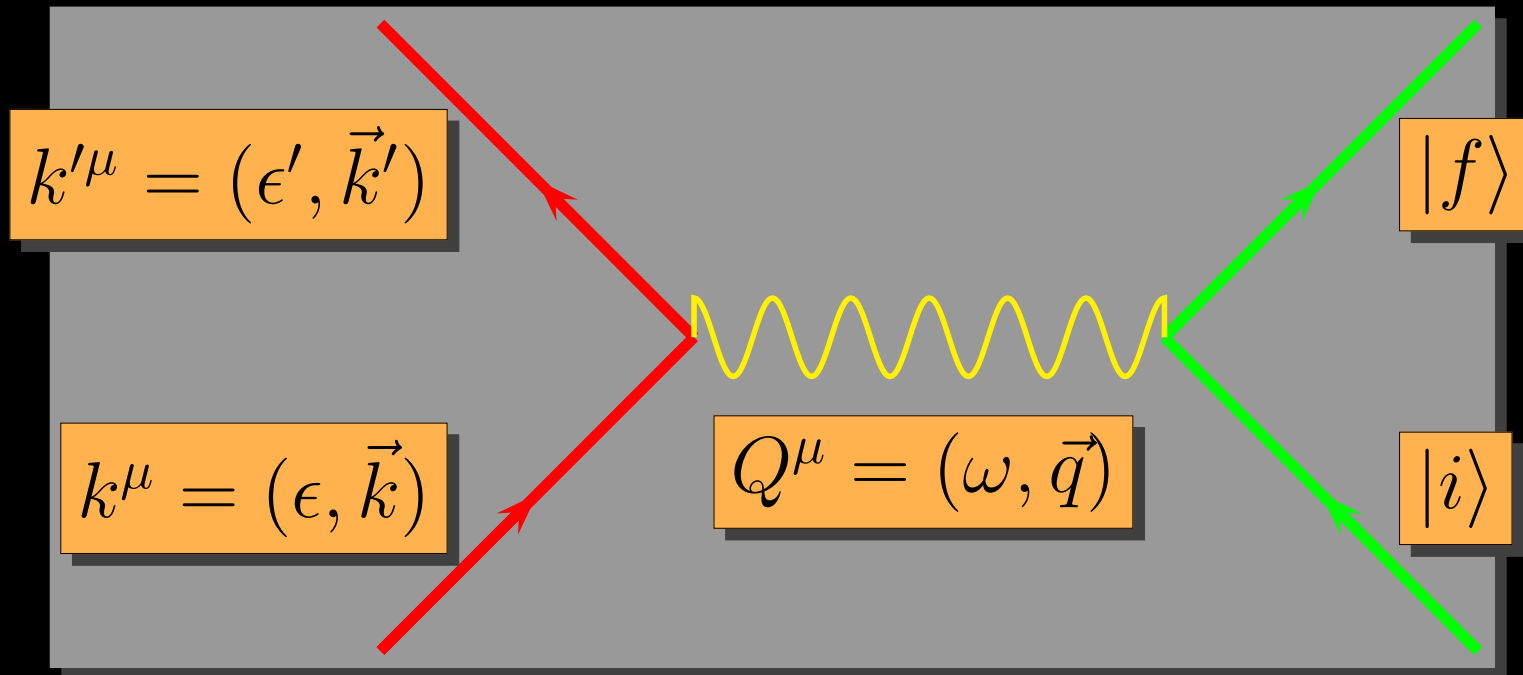
1 Lepton scattering



1 Lepton scattering



Kinematics



$$Q^2 = \omega^2 - q^2 < 0$$

Adimensional variables

$$\lambda = \frac{\omega}{2m_N} \quad \kappa = \frac{q}{2m_N} \quad \tau = \kappa^2 - \lambda^2$$

(e, e') formalism

$$\frac{d\sigma}{d\epsilon' d\Omega'} = \sigma_{Mott} (v_L R_L + v_T R_T)$$

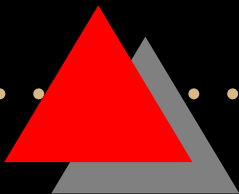


(e, e') formalism

$v_L, v_T \longrightarrow$ Kinematical factors

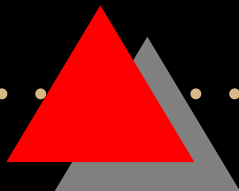
$$\frac{d\sigma}{d\epsilon' d\Omega'} = \sigma_{Mott} (v_L R_L + v_T R_T)$$

$\sigma_{Mott} \longrightarrow$ Mott cross section



(e, e') formalism

$$\frac{d\sigma}{d\epsilon' d\Omega'} = \sigma_{Mott} (v_L R_L + v_T R_T)$$



(ν_l, l^-) formalism

$$\frac{d\sigma}{d\Omega' d\epsilon'} = \sigma_0 \left[\widehat{V}_{CC} R_{CC} + 2\widehat{V}_{CL} R_{CL} + \widehat{V}_{LL} R_{LL} + \widehat{V}_T R_T + 2\widehat{V}_{T'} R_{T'} \right]$$

(ν_l, l^-) formalism

$$\frac{d\sigma}{d\Omega' d\epsilon'} = \sigma_0 \left[\widehat{V}_{CC} R_{CC} + 2\widehat{V}_{CL} R_{CL} + \widehat{V}_{LL} R_{LL} + \widehat{V}_T R_T + 2\widehat{V}_{T'} R_{T'} \right]$$

$\sigma_0 \rightarrow$ similar to σ_{Mott} .

$\widehat{V}_K \rightarrow$ Kinematical factors

(ν_l, l^-) formalism

$$\frac{d\sigma}{d\Omega' d\epsilon'} = \sigma_0 \left[\widehat{V}_{CC} R_{CC} + 2\widehat{V}_{CL} R_{CL} + \widehat{V}_{LL} R_{LL} + \widehat{V}_T R_T + 2\widehat{V}_{T'} R_{T'} \right]$$

Hadronic Tensor

$$W^{\mu\nu}(q, \omega) = \overline{\sum_{fi}} \delta(E_f - E_i - \omega) \langle f | J^\mu(Q) | i \rangle^* \langle f | J^\nu(Q) | i \rangle .$$

$J^\mu(Q)$: Charge operator

- Electromagnetic current for (e, e')
- Weak charged current for (ν_l, l^-)



Single-nucleon current

Electromagnetic current

$$j^\mu(\mathbf{p}', \mathbf{p}) = \bar{u}(\mathbf{p}') \left[2F_1 \gamma^\mu + i \frac{F_2}{m_N} \sigma^{\mu\nu} Q_\nu \right] u(\mathbf{p})$$

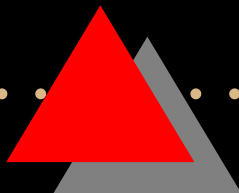
Weak CC current $j^\mu = j_V^\mu - j_A^\mu$.

$$j_V^\mu(\mathbf{p}', \mathbf{p}) = \bar{u}(\mathbf{p}') \left[2F_1^V \gamma^\mu + i \frac{F_2^V}{m_N} \sigma^{\mu\nu} Q_\nu \right] u(\mathbf{p})$$

← Vector

$$j_A^\mu(\mathbf{p}', \mathbf{p}) = \bar{u}(\mathbf{p}') \left[G_A \gamma^\mu + G_P \frac{Q^\mu}{2m_N} \right] \gamma^5 u(\mathbf{p})$$

← Axial-Vector



2 Scaling

RFG (Relativistic Fermi gas)

$$R_K = G_K f_{RFG}(\psi)$$

Functions G_K from the RFG for electrons ($K = L, T$) and neutrinos $K = CC, CL, LL, T, T'$.

Scaling function in the RFG

$$f_{RFG}(\psi) = \frac{3}{4}(1 - \psi^2)\theta(1 - \psi^2)$$

Scaling variable:

$$\psi = \frac{1}{\sqrt{\xi_F}} \frac{\lambda - \tau}{\sqrt{(1 + \lambda)\tau + \kappa\sqrt{\tau(1 + \tau)}}$$

(e, e') experimental scaling function

$$f(\psi') = \frac{\left(\frac{d\sigma}{d\Omega' d\epsilon'} \right)_{exp}}{\sigma_{Mott}(v_L G_L + v_T G_T)}$$

shifted $\longrightarrow \psi' = \frac{1}{\sqrt{\xi_F}} \frac{\lambda' - \tau'}{\sqrt{(1 + \lambda')\tau' + \kappa\sqrt{\tau'(1 + \tau')}}}$

$$\lambda' = (\omega - E_s)/2m_N, \quad \tau' = \kappa^2 - \lambda'^2$$

k_F y E_s are fitted to the data

$$f_L = \frac{R_L}{G_L} \text{Longitudinal} \quad f_T = \frac{R_T}{G_T} \text{Transverse}$$

Superscaling

- Plot the experimental $f(\psi')$ versus ψ' for different kinematics and nuclei
- Fit E_s and k_F to get scaling (one universal scaling function)

no q
dependence

1st kind
scaling

no A
dependence

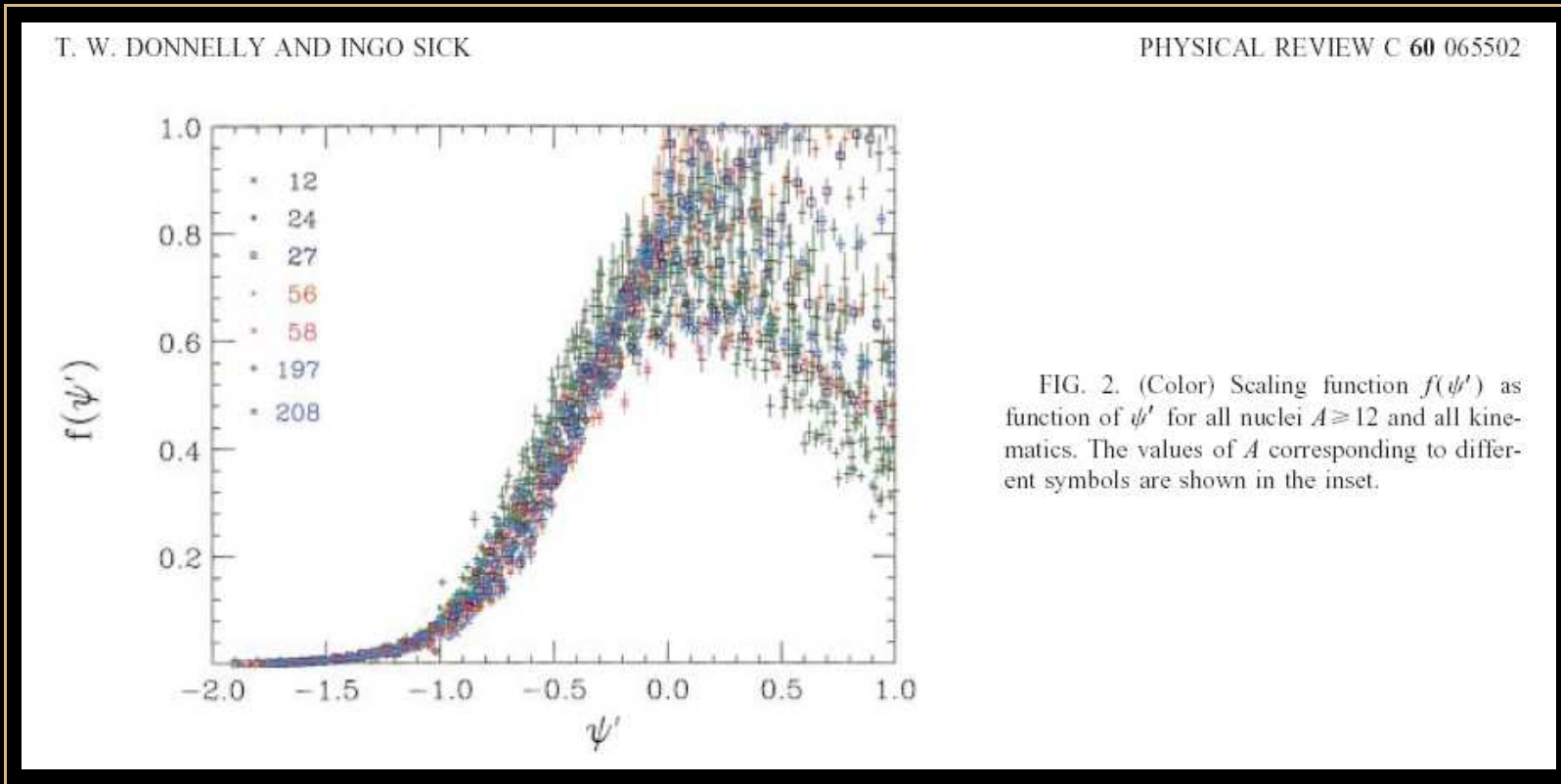
2nd kind
scaling

Superscaling



Scaling in the QE peak

Summary of past work by Donnelly & Sick PRC 60 (1999)



Scaling in the QE peak

Summary of past work by Donnelly & Sick PRC 60 (1999)

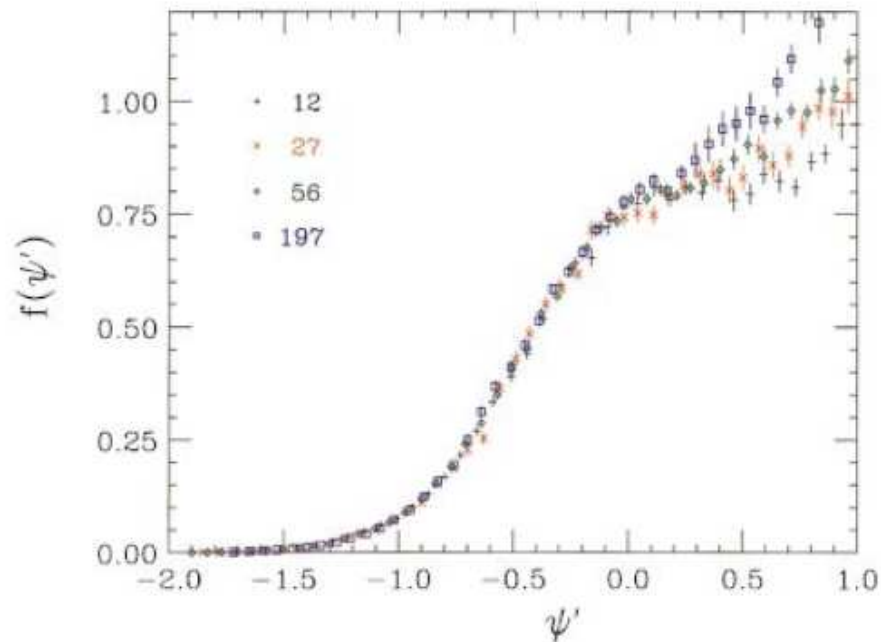
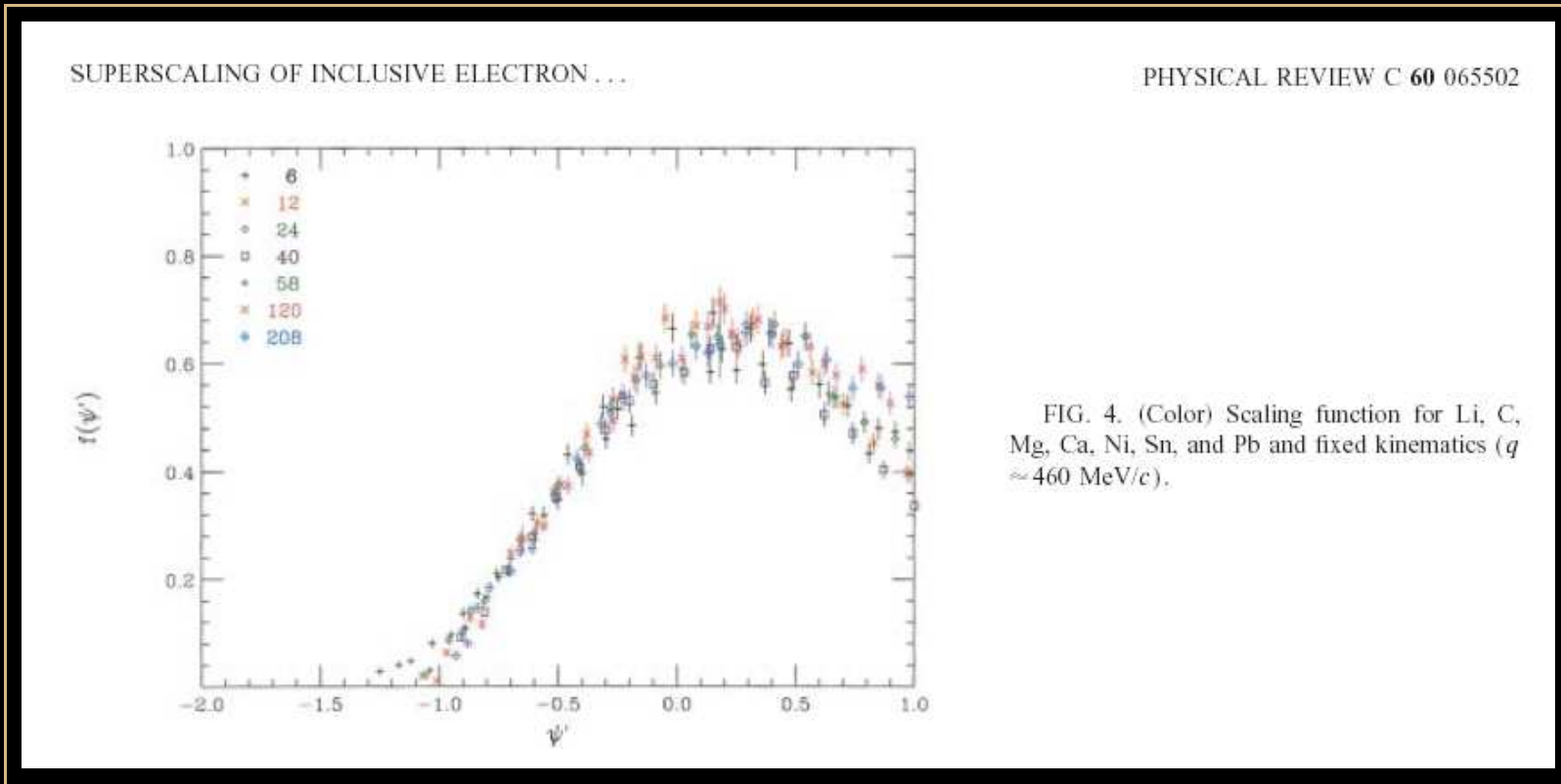


FIG. 3. (Color) Scaling function for C, Al, Fe, and Au and fixed kinematics ($q \approx 1000$ MeV/c).

Scaling in the QE peak

Summary of past work by Donnelly & Sick PRC 60 (1999)



Scaling in the QE peak

Summary of past work by Donnelly & Sick PRC 60 (1999)

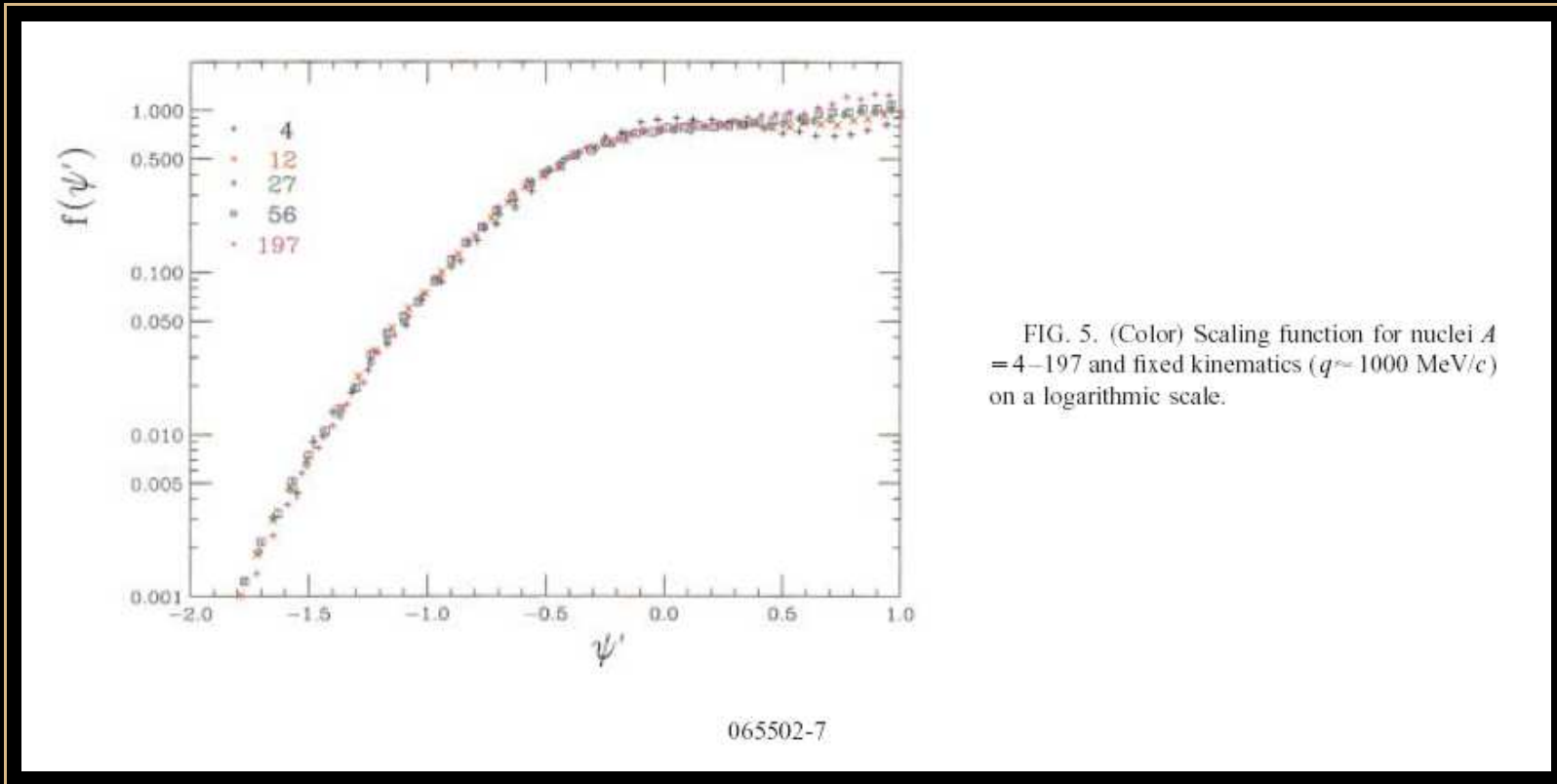
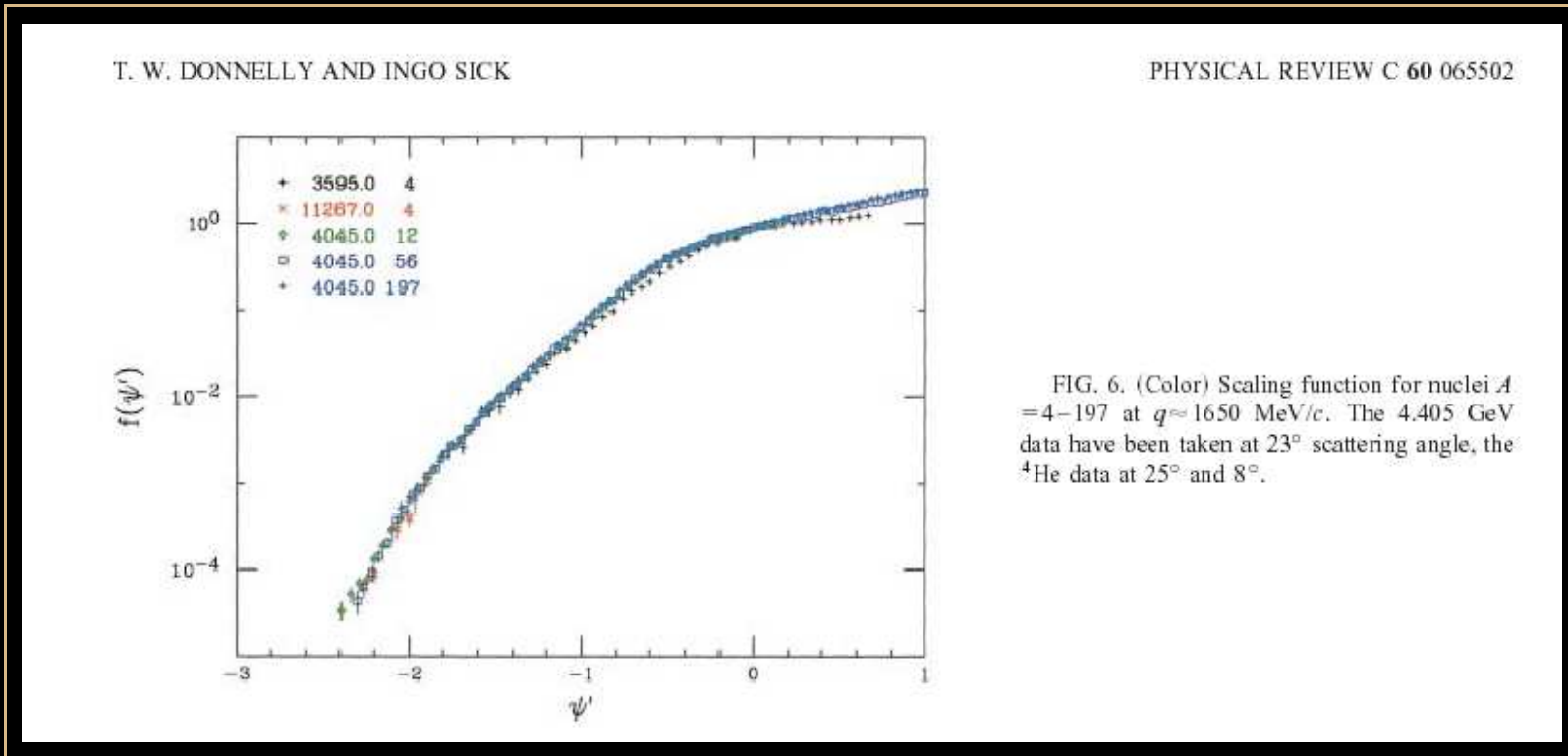


FIG. 5. (Color) Scaling function for nuclei $A = 4-197$ and fixed kinematics ($q \approx 1000$ MeV/c) on a logarithmic scale.

Scaling in the QE peak

Summary of past work by Donnelly & Sick PRC 60 (1999)



Scaling in the QE peak

Summary of past work by Donnelly & Sick PRC 60 (1999)

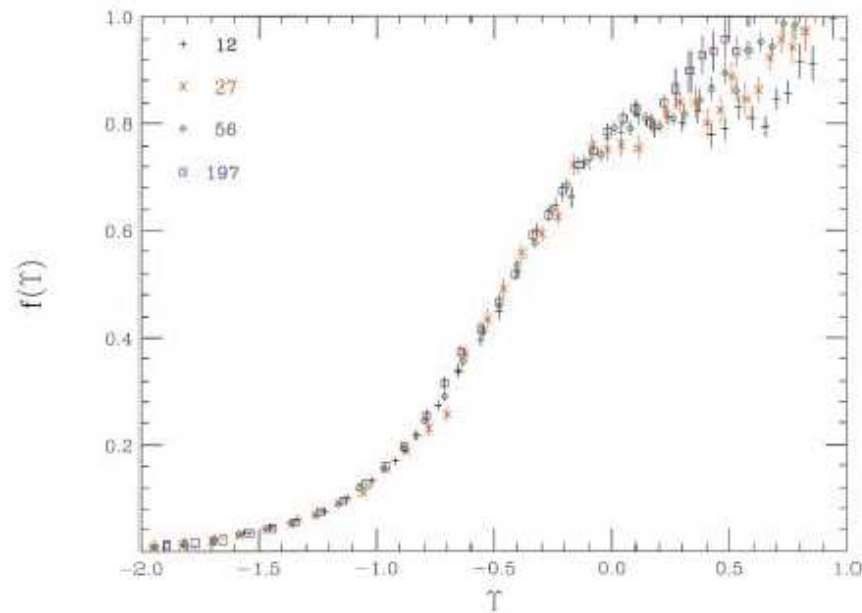


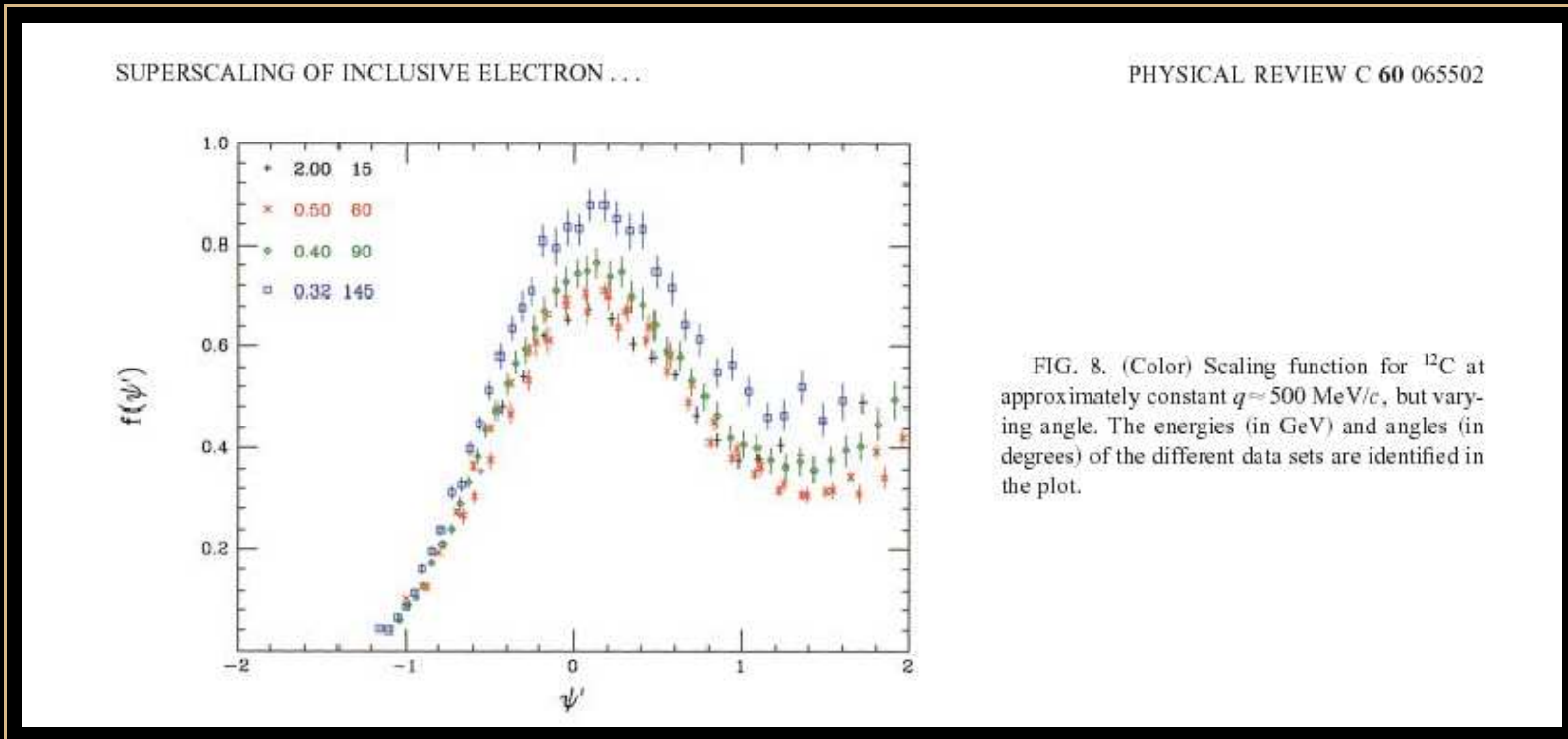
FIG. 7. (Color) Scaling function $f(Y)$ for nuclei $A = 12-197$ at 3.6 GeV energy and 16° scattering angle as a function of the scaling variable Y .

065502-8



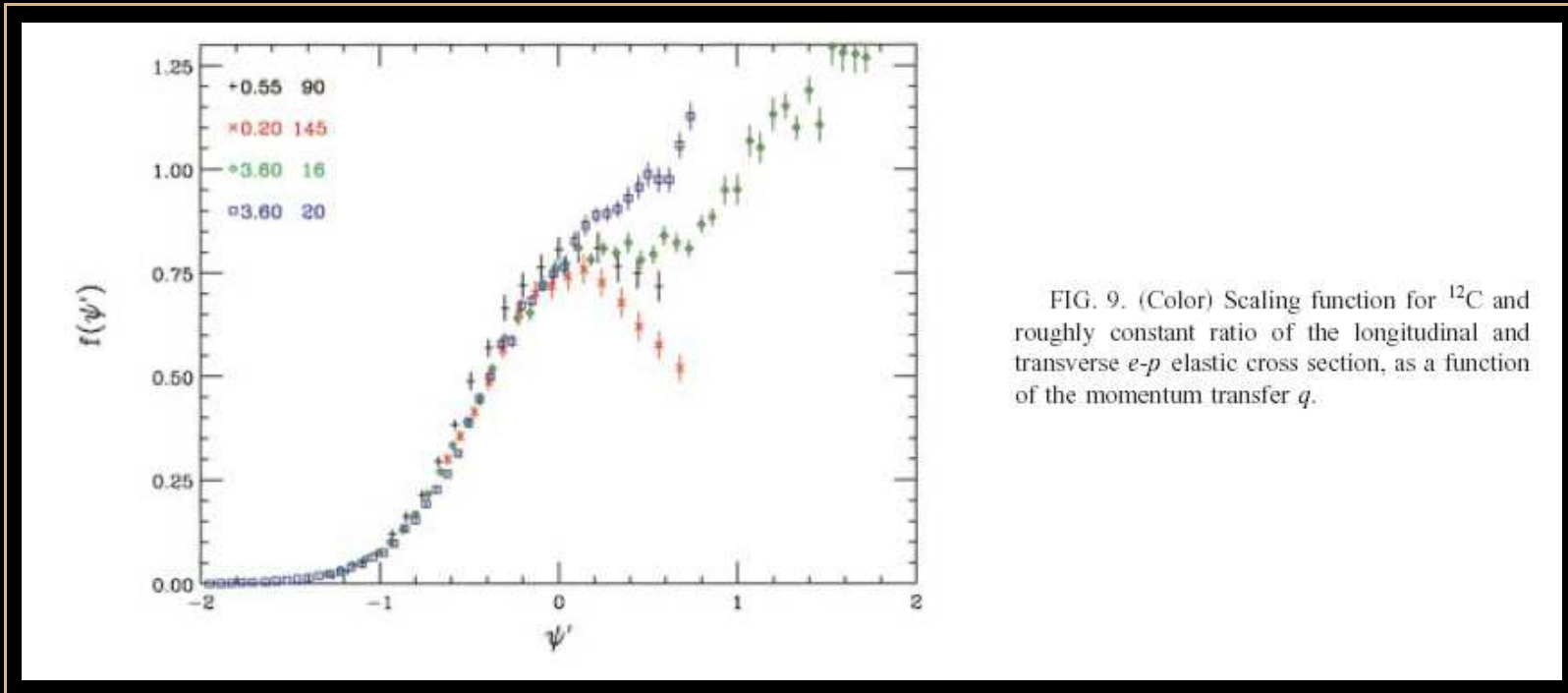
Scaling in the QE peak

Summary of past work by Donnelly & Sick PRC 60 (1999)



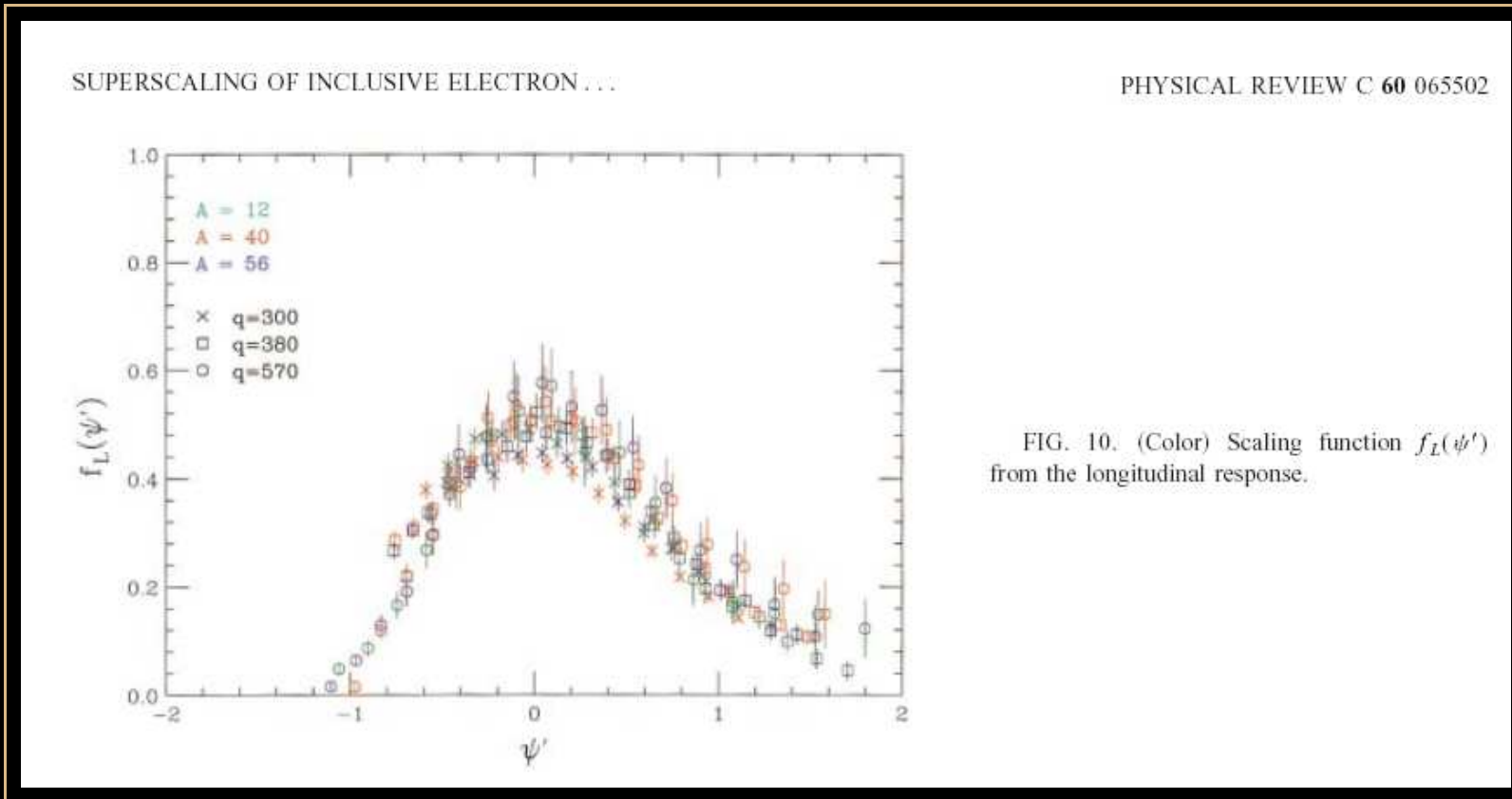
Scaling in the QE peak

Summary of past work by Donnelly & Sick PRC 60 (1999)



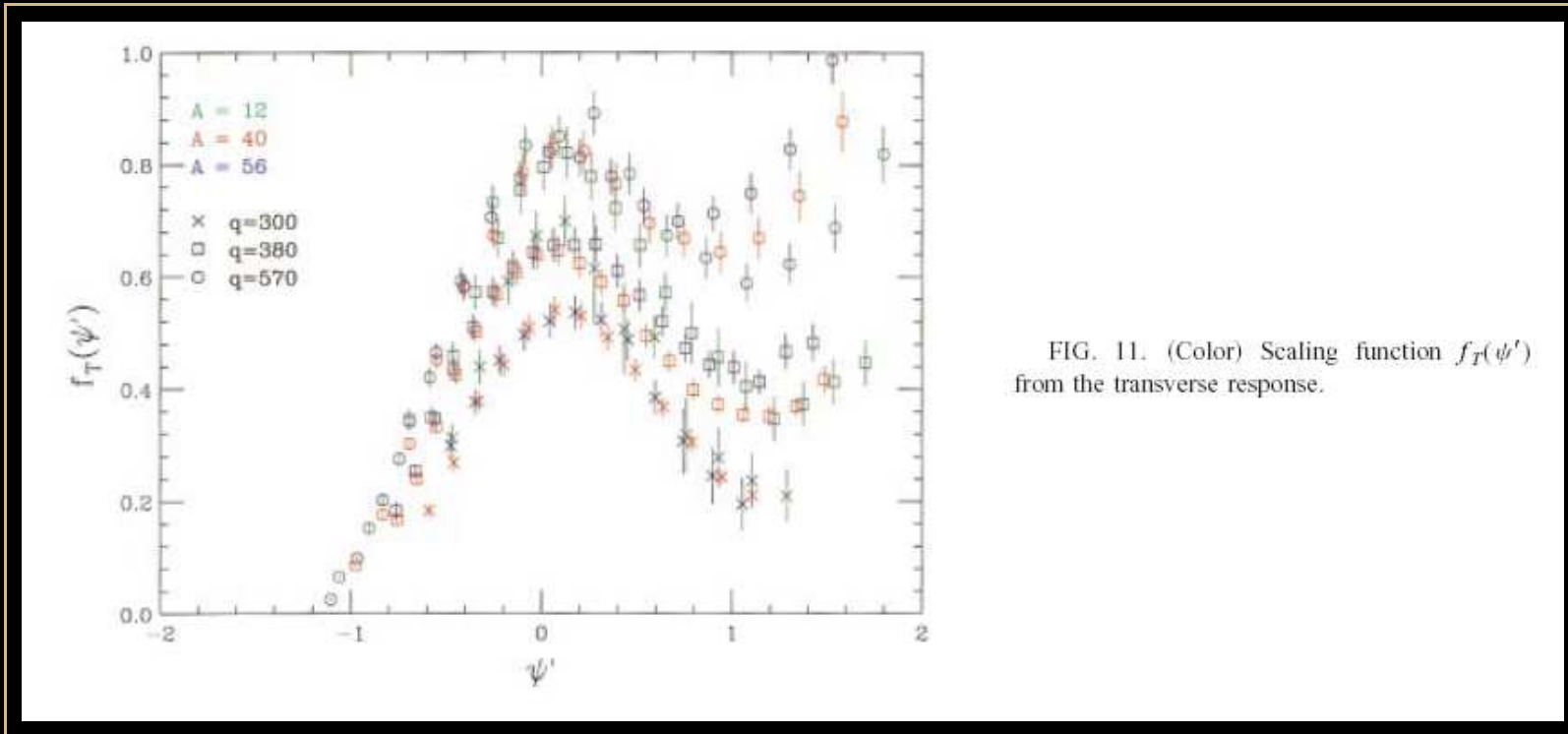
Scaling in the QE peak

Summary of past work by Donnelly & Sick PRC 60 (1999)



Scaling in the QE peak

Summary of past work by Donnelly & Sick PRC 60 (1999)



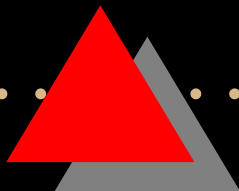
Scaling properties of data

- Good 1st-kind scaling below the QE peak (scaling region)



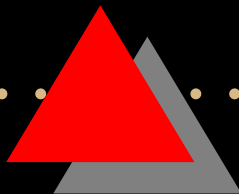
Scaling properties of data

- Good 1st-kind scaling below the QE peak (scaling region)
- Above the peak the scaling is broken (Δ region)



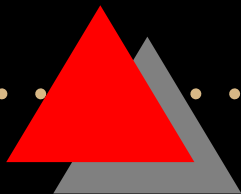
Scaling properties of data

- Good 1st-kind scaling below the QE peak (scaling region)
- Above the peak the scaling is broken (Δ region)
- Scaling of the 2nd-kind works well in the scaling region



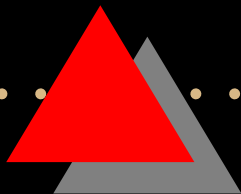
Scaling properties of data

- Good 1st-kind scaling below the QE peak (scaling region)
- Above the peak the scaling is broken (Δ region)
- Scaling of the 2nd-kind works well in the scaling region
- The longitudinal response appears to superscale

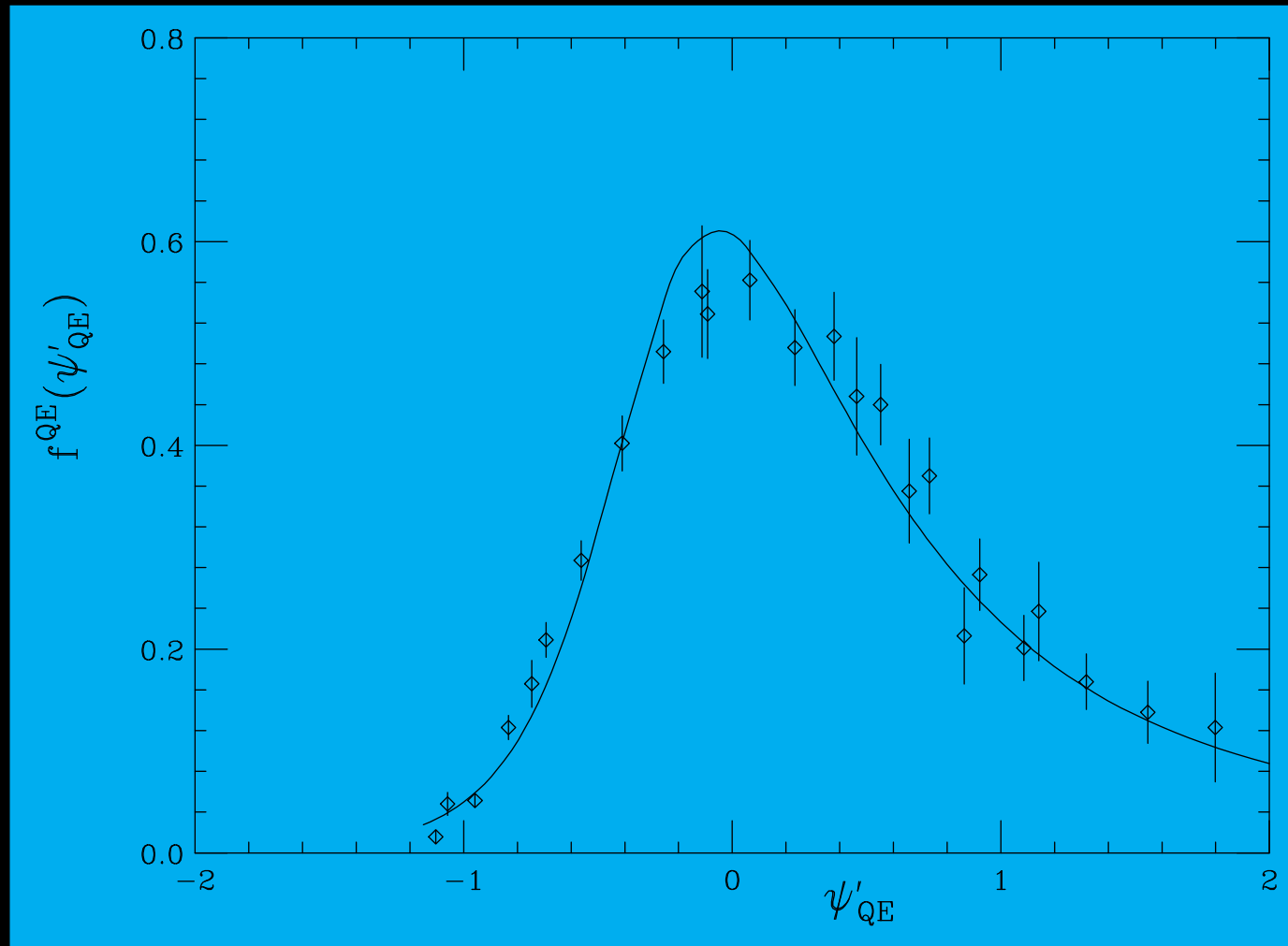


Scaling properties of data

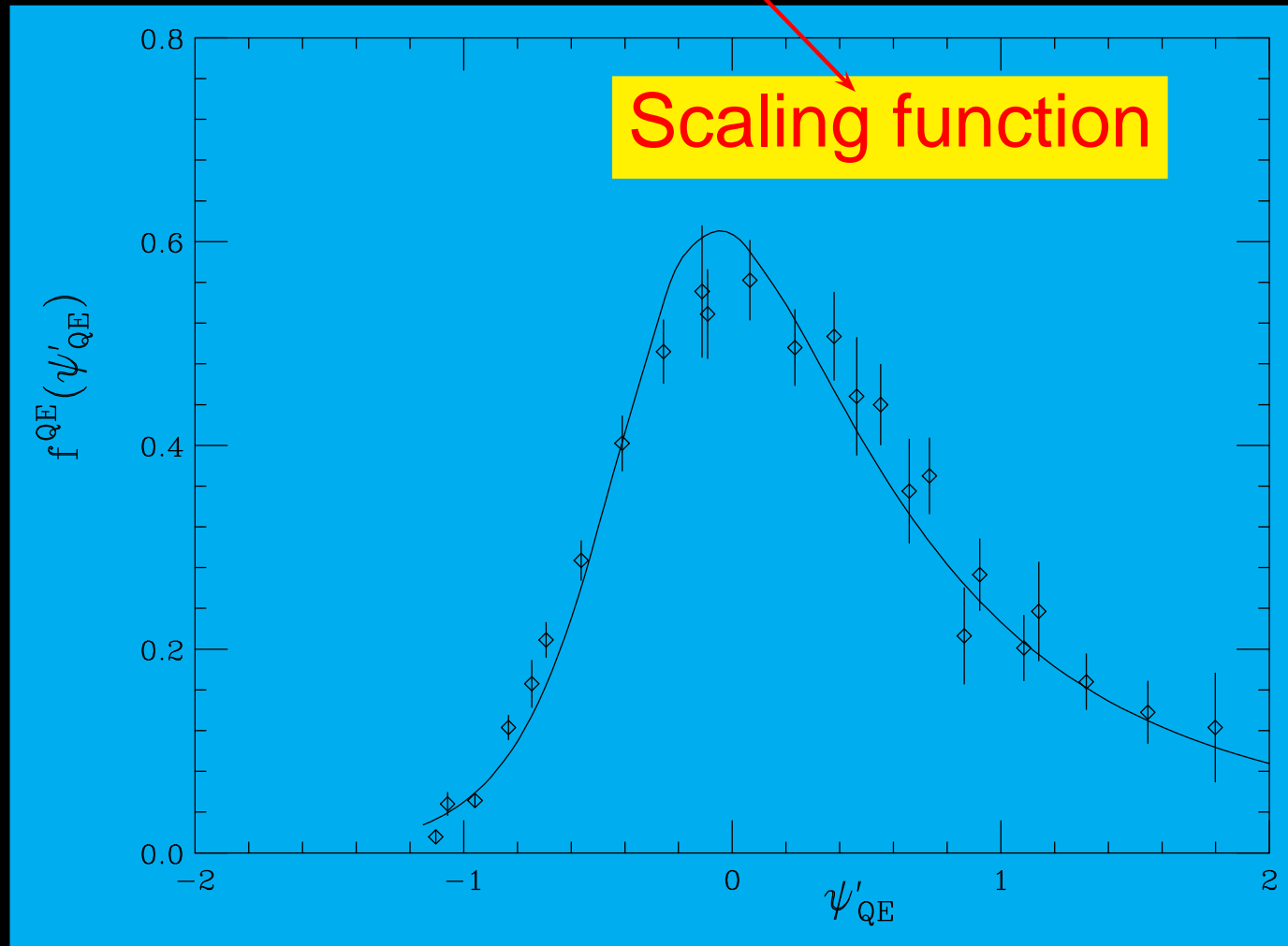
- Good 1st-kind scaling below the QE peak (scaling region)
- Above the peak the scaling is broken (Δ region)
- Scaling of the 2nd-kind works well in the scaling region
- The longitudinal response appears to superscale
- Scaling violations reside in the transverse response,



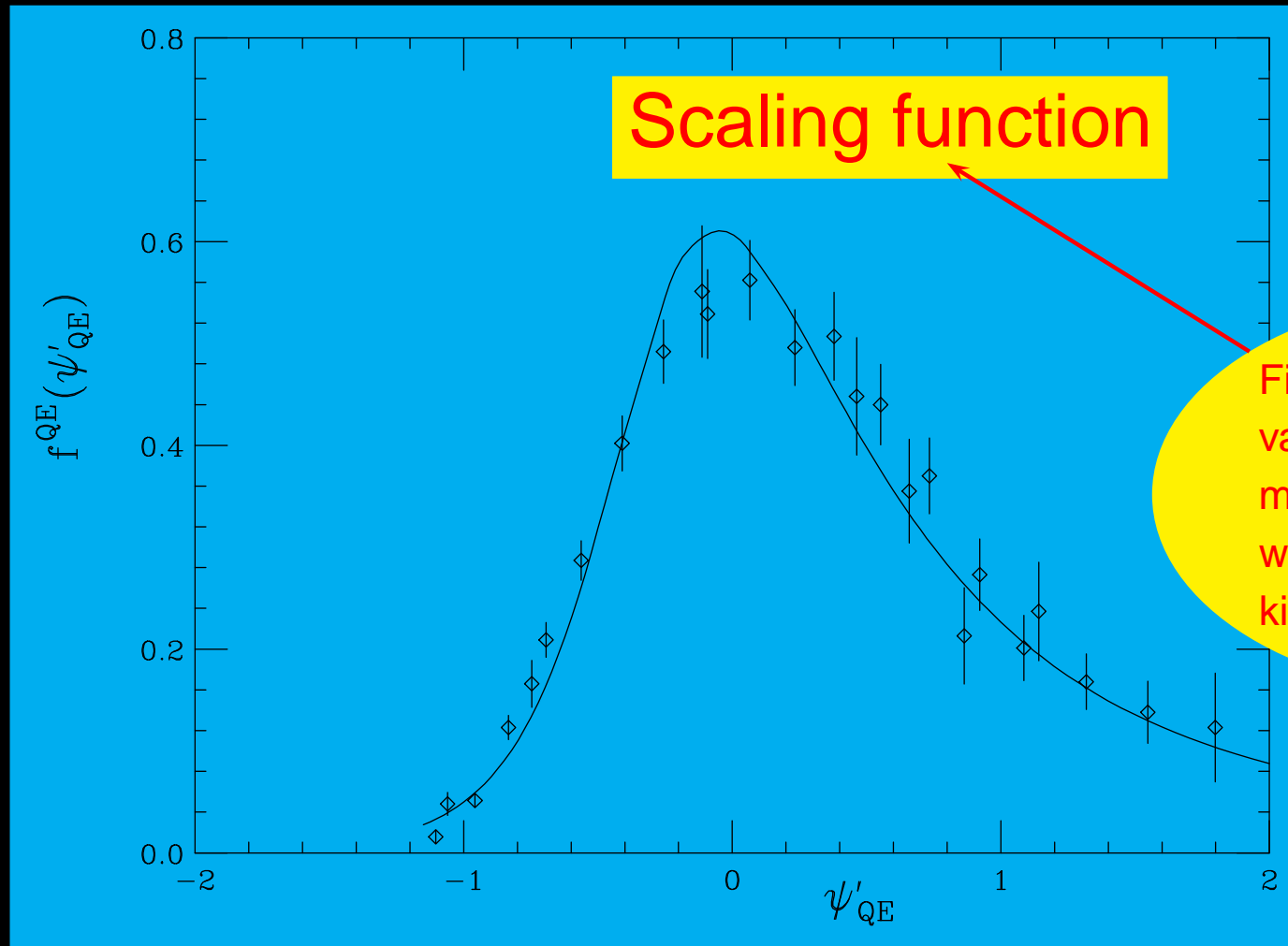
Fit in the Quasi-elastic peak



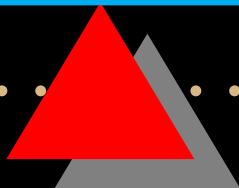
Fit in the Quasi-elastic peak



Fit in the Quasi-elastic peak

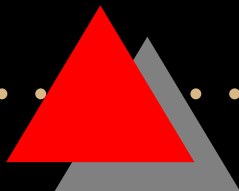


Fitted to the set of f_L values for the higher momentum transfer where scaling of the first kind is seen to occur



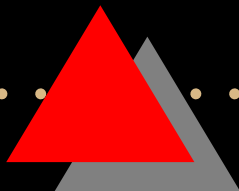
SuSA (Super Scaling Analysis)

- Using the experimental (e, e') scaling function to predict neutrino cross sections



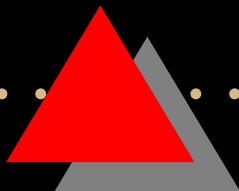
SuSA (Super Scaling Analysis)

- Using the experimental (e, e') scaling function to predict neutrino cross sections
- Use the RFG equations to compute the (ν_l, l^-) response functions with the substitution $f_{RFG}(\psi) \longrightarrow f_{exp}(\psi)$



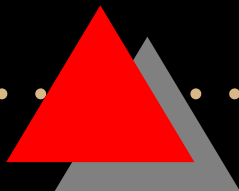
SuSA (*Super Scaling Analysis*)

- Using the experimental (e, e') scaling function to predict neutrino cross sections
- Use the RFG equations to compute the (ν_l, l^-) response functions with the substitution $f_{RFG}(\psi) \longrightarrow f_{exp}(\psi)$
- Needed to justify theoretically the validity of SuSA



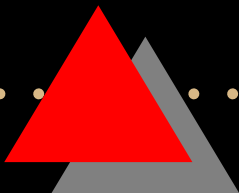
3 *The semirelativistic shell model*

- Study the scaling properties in realistic models



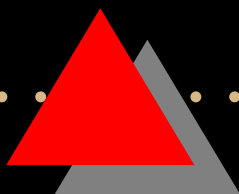
3 *The semirelativistic shell model*

- Study the scaling properties in realistic models
- Estimate the validity range of SuSA



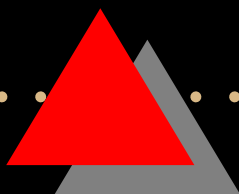
3 *The semirelativistic shell model*

- Study the scaling properties in realistic models
- Estimate the validity range of SuSA
- Include relativistic effects in the model



3 *The semirelativistic shell model*

- Study the scaling properties in realistic models
- Estimate the validity range of SuSA
- Include relativistic effects in the model
- Compare with the experimental scaling function



The continuum shell-model (CSM)

- Closed-shell nuclei ^{12}C , ^{16}O and ^{40}Ca ,
- Initial state $|i\rangle$: Slater determinant with all shells occupied.
- Impulse approximation: final states are particle-hole excitations coupled to total angular momentum

$$|f\rangle = |(ph^{-1})J\rangle$$

- Single hole wave function $|h\rangle = |\epsilon_h l_h j_h\rangle$
- Single particle wave function $|p\rangle = |\epsilon_p l_p j_p\rangle$
- Obtained by solving the Schrödinger equation

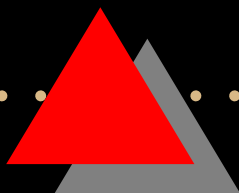
Woods-Saxon potential

$$V(r) = -V_0 f(r, R_0, a_0) + \frac{V_{ls}}{m_{\pi}^2 r} \frac{df(r, R_0, a_0)}{dr} \mathbf{l} \cdot \boldsymbol{\sigma} + V_C(r)$$

$$f(r, R, a) = \frac{1}{1 + e^{(r-R)/a}}$$

$V_C(r)$: Coulomb potential.

	V_0^p	V_{LS}^p	V_0^n	V_{LS}^n	r_0	a_0
^{12}C	62.0	3.20	60.00	3.15	1.25	0.57
^{16}O	52.5	7.00	52.50	6.54	1.27	0.53
^{40}Ca	57.5	11.11	55.00	8.50	1.20	0.53



The SR approach

A

EXPAND THE RELATIVISTIC SINGLE-NUCLEON CURRENT

$$j^\mu(\vec{p}', \vec{p}) = \bar{u}(\vec{p}') \Gamma^\mu(Q) u(\vec{p})$$

in powers of $\vec{\eta} = \vec{p}'/m_N$. to first order $O(\eta)$

Not expand in \vec{p}'/m_N .

$\implies q, \omega$ can be large

Relativistic kinematics

B

USE RELATIVISTIC KINEMATICS.

- The energy transfer is the difference between the (non-relativistic) single-particle energies of particle and hole $\omega = \epsilon_p - \epsilon_h$.
- The relativistic kinematics are taken into account by the substitution

$$\epsilon_p \rightarrow \epsilon_p(1 + \epsilon_p/2m_N)$$

as the eigenvalue of the Schrödinger equation for the particle

The SR vector current

$$J_V^0 = \xi_0 + i\xi'_0(\boldsymbol{\kappa} \times \boldsymbol{\eta}) \cdot \boldsymbol{\sigma}$$

$$\mathbf{J}_V^\perp = \xi_1 \boldsymbol{\eta}^\perp + i\xi'_1 \boldsymbol{\sigma} \times \boldsymbol{\kappa},$$

(q, ω) -dependent factors:

$$\xi_0 = \frac{\kappa}{\sqrt{\tau}} 2G_E^V, \quad \xi'_0 = \frac{2G_M^V - G_E^V}{\sqrt{1 + \tau}}$$

$$\xi'_1 = 2G_M^V \frac{\sqrt{\tau}}{\kappa}, \quad \xi_1 = 2G_E^V \frac{\sqrt{\tau}}{\kappa}$$

provide the required relativistic behavior.

The longitudinal component is given from vector current conservation, $J_V^3 = \frac{\lambda}{\kappa} J_V^0$.

The SR axial-vector current

$$\mathbf{J}_A^\perp = \zeta_1' \boldsymbol{\sigma}^\perp, \quad \zeta_1' = \sqrt{1 + \tau G_A}.$$

Transverse

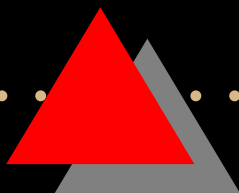
Neglect the terms of order $O(\eta)$

$$J_A^0 = \zeta_0' \boldsymbol{\kappa} \cdot \boldsymbol{\sigma} + \zeta_0'' \boldsymbol{\eta}^\perp \cdot \boldsymbol{\sigma}$$

Time component

$$J_A^z = \zeta_3' \boldsymbol{\kappa} \cdot \boldsymbol{\sigma} + \zeta_3'' \boldsymbol{\eta}^\perp \cdot \boldsymbol{\sigma},$$

Longitudinal component



The SR axial-vector current

$$\mathbf{J}_A^\perp = \zeta'_1 \boldsymbol{\sigma}^\perp, \quad \zeta'_1 = \sqrt{1 + \tau} G_A.$$

Transverse

Neglect the terms of order $O(\eta)$

$$J_A^0 = \zeta'_0 \boldsymbol{\kappa} \cdot \boldsymbol{\sigma} + \zeta''_0 \boldsymbol{\eta}^\perp \cdot \boldsymbol{\sigma}$$

Time component

$$J_A^z = \zeta'_3 \boldsymbol{\kappa} \cdot \boldsymbol{\sigma} + \zeta''_3 \boldsymbol{\eta}^\perp \cdot \boldsymbol{\sigma},$$

Longitudinal component

$$\zeta'_0 = \frac{1}{\sqrt{\tau}} \frac{\lambda}{\kappa} G'_A, \quad \zeta''_0 = \frac{\kappa}{\sqrt{\tau}} \left[G_A - \frac{\lambda^2}{\kappa^2 + \kappa \sqrt{\tau(\tau + 1)}} G'_A \right]$$

$$\zeta'_3 = \frac{1}{\sqrt{\tau}} G'_A, \quad \zeta''_3 = \frac{\lambda}{\sqrt{\tau}} \left[G_A - \frac{\kappa}{\kappa + \sqrt{\tau(\tau + 1)}} G'_A \right]$$

$G'_A = G_A - \tau G_P$ small due to cancellations

The $O(\eta)$ term, proportional to $\vec{\eta}^\perp \cdot \vec{\sigma}$ is dominant

Multipole expansion

Multipole components of the current operator: Coulomb (C), longitudinal (L), transverse electric (E) and transverse magnetic (M) operators

$$\hat{C}_{J_0}(q) = \int d^3r j_J(qr) Y_{J_0}(\hat{\mathbf{r}}) J_0(\mathbf{r})$$

$$\hat{L}_{J_0}(q) = \frac{i}{q} \int d^3r \nabla [j_J(qr) Y_{J_0}(\hat{\mathbf{r}})] \cdot \mathbf{J}(\mathbf{r})$$

$$\hat{E}_{Jm}(q) = \frac{1}{q} \int d^3r \nabla \times [j_J(qr) \mathbf{Y}_{JJm}(\hat{\mathbf{r}})] \cdot \mathbf{J}(\mathbf{r})$$

$$\hat{M}_{Jm}(q) = \int d^3r j_J(qr) \mathbf{Y}_{JJm}(\hat{\mathbf{r}}) \cdot \mathbf{J}(\mathbf{r}) ,$$

$j_J(qr)$: spherical Bessel Function

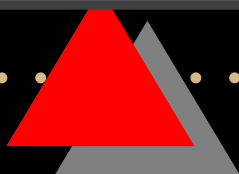
$\mathbf{Y}_{JJm}(\hat{\mathbf{r}})$: vector spherical harmonic

Multipole matrix elements

- Index to label the quantum numbers $\alpha = (h, l_p, j_p, J)$
- C , L , E and M multipole matrix elements of vector and axial-vector currents:

$$\begin{aligned}
 C_{\alpha}^V + iC_{\alpha}^A &= \langle f || \hat{C}_J(q) || i \rangle \\
 L_{\alpha}^V + iL_{\alpha}^A &= \langle f || \hat{L}_J(q) || i \rangle \\
 E_{\alpha}^V + iE_{\alpha}^A &= \langle f || \hat{E}_J(q) || i \rangle \\
 -iM_{\alpha}^V - M_{\alpha}^A &= \langle f || \hat{M}_J(q) || i \rangle
 \end{aligned}$$

- These are computed in terms of the radial wave functions using Racah algebra



Multipole expansion of response functions

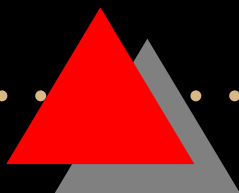
$$R_{CC} = 4\pi \sum_{\alpha} (|C_{\alpha}^V|^2 + |C_{\alpha}^A|^2)$$

$$R_{CL} = 2\pi \sum_{\alpha} (C_{\alpha}^{V*} L_{\alpha}^V + C_{\alpha}^V L_{\alpha}^{V*} + C_{\alpha}^{A*} L_{\alpha}^A + C_{\alpha}^A L_{\alpha}^{A*})$$

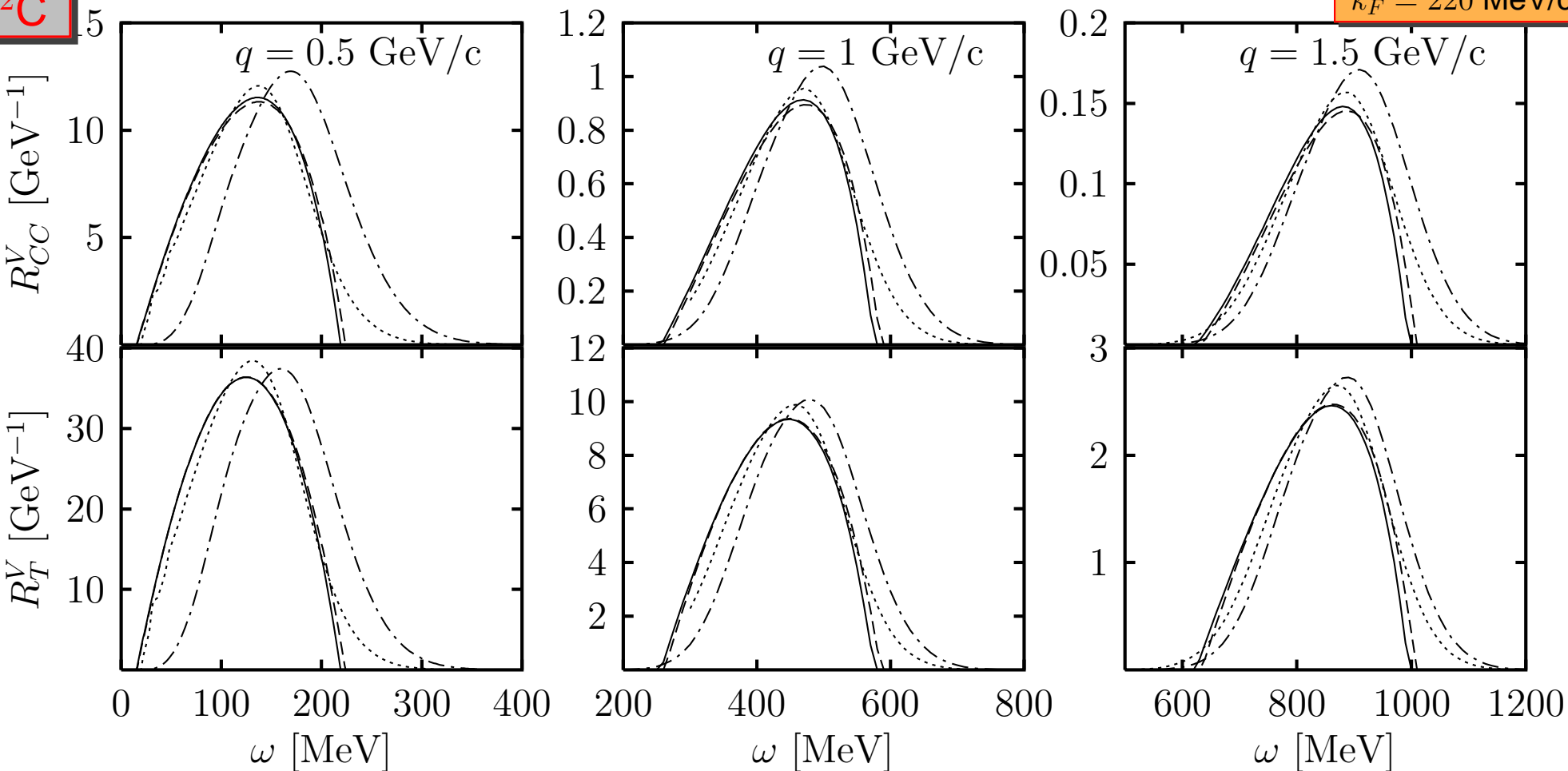
$$R_{LL} = 4\pi \sum_{\alpha} (|L_{\alpha}^V|^2 + |L_{\alpha}^A|^2)$$

$$R_T = 4\pi \sum_{\alpha} (|E_{\alpha}^V|^2 + |M_{\alpha}^V|^2 + |E_{\alpha}^A|^2 + |M_{\alpha}^A|^2)$$

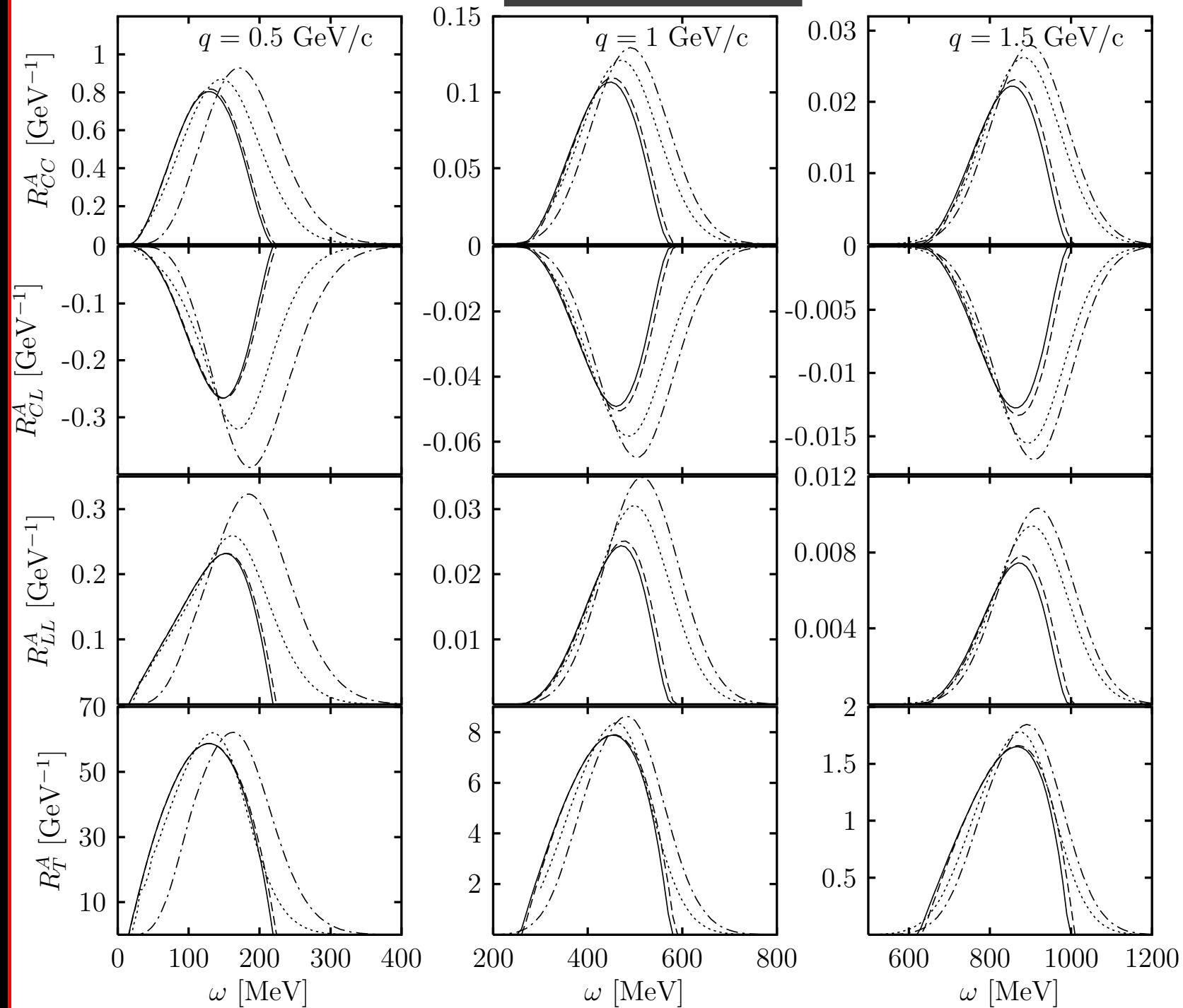
$$R_{T'} = 2\pi \sum_{\alpha} (E_{\alpha}^{V*} M_{\alpha}^A + E_{\alpha}^V M_{\alpha}^{A*} + E_{\alpha}^{A*} M_{\alpha}^V + E_{\alpha}^A M_{\alpha}^{V*}) ,$$

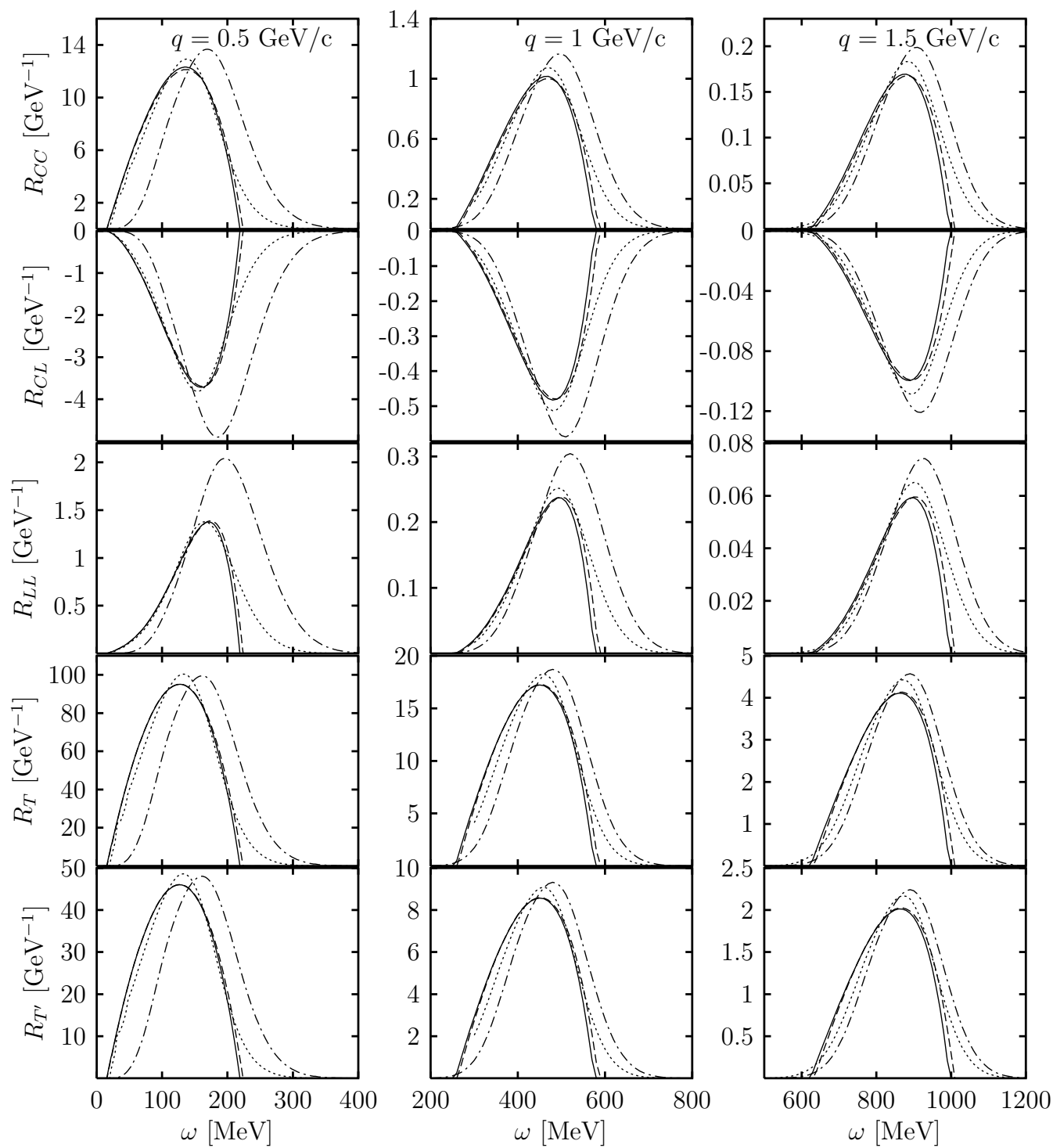


Test of the SR approach: V responses

 ^{22}C $k_F = 220 \text{ MeV}/c$ 

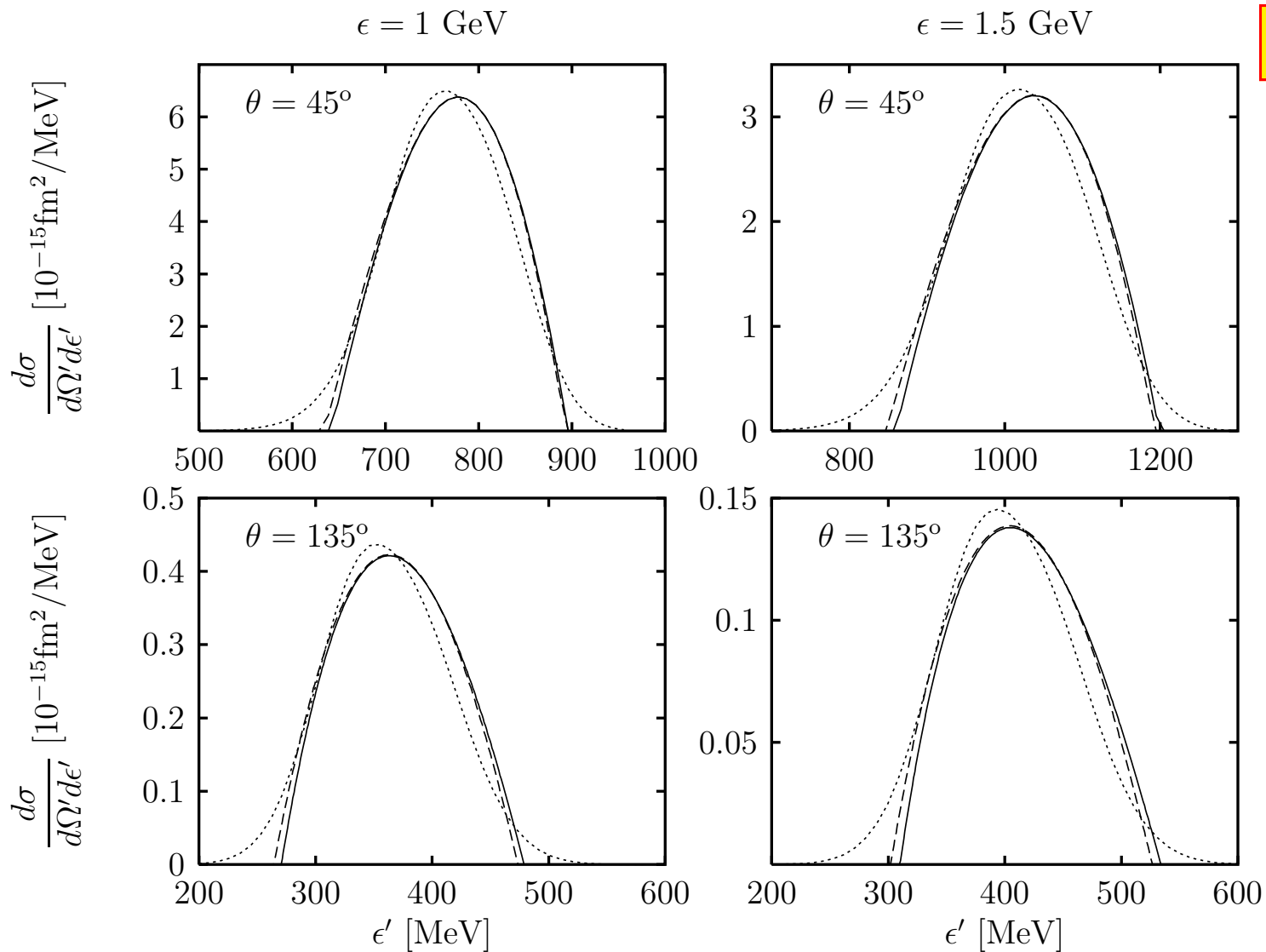
Solid lines: RFG Dashed lines: SRFG
 Dotted: CSM Dot-dashed: PWIA.





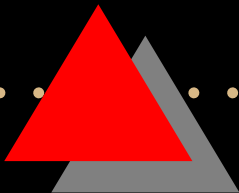
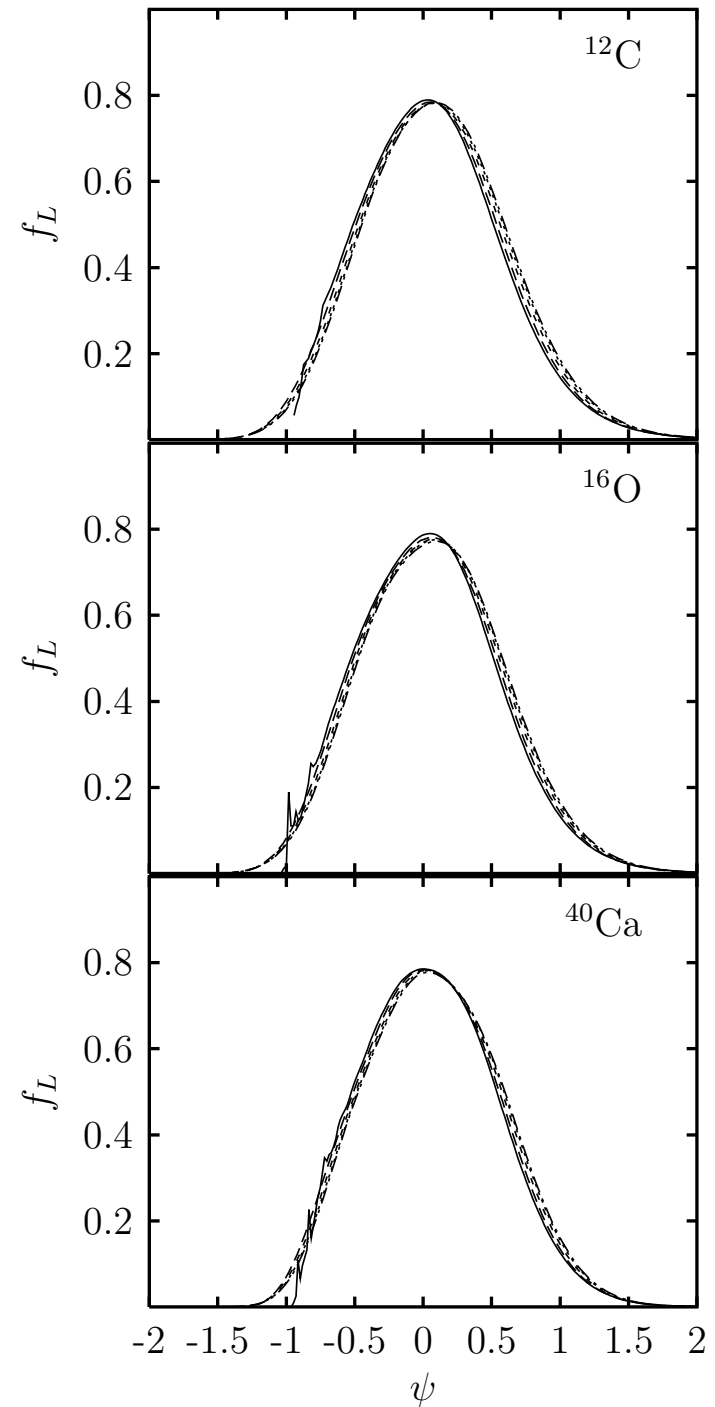
Total responses

Test of the SR approach: Cross section

 $^{12}\text{C}(\nu_{\mu}, \mu^{-})$


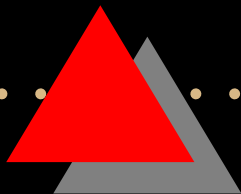
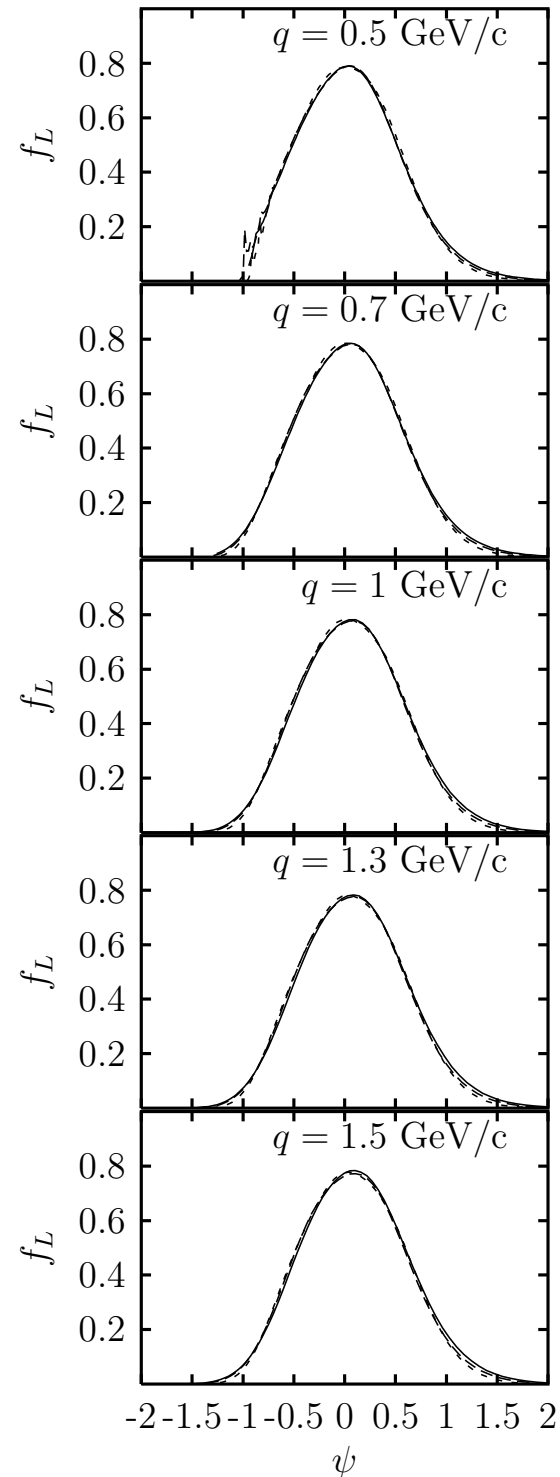
Scaling of the first kind

Curves for
 $q = 0.5, 0.7, 1, 1.3, 1.5$ GeV
collapse into one



Scaling of the second kind

Curves for
 ^{12}C , ^{16}O and ^{40}Ca
collapse into one



Superscaling

Scaling of the first kind

+ Scaling of the second kind

= Superscaling
in the CSM

Improvement of the FSI

C

DEB+D POTENTIAL (DIRAC-EQUATION-BASED PLUS DARWIN TERM) EN EL ESTADO FINAL:

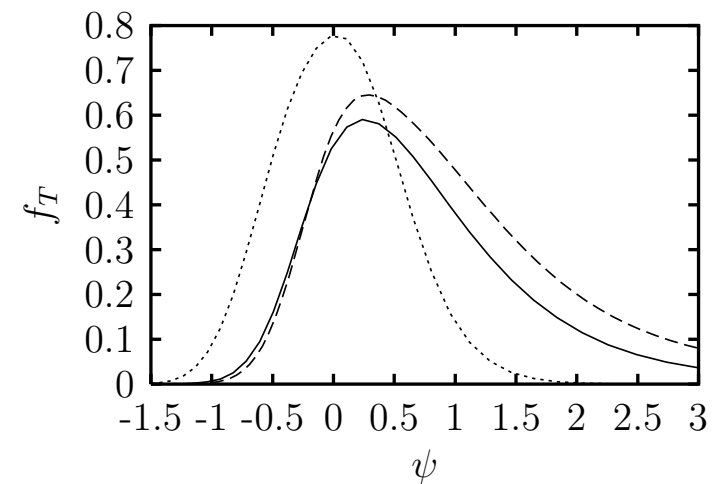
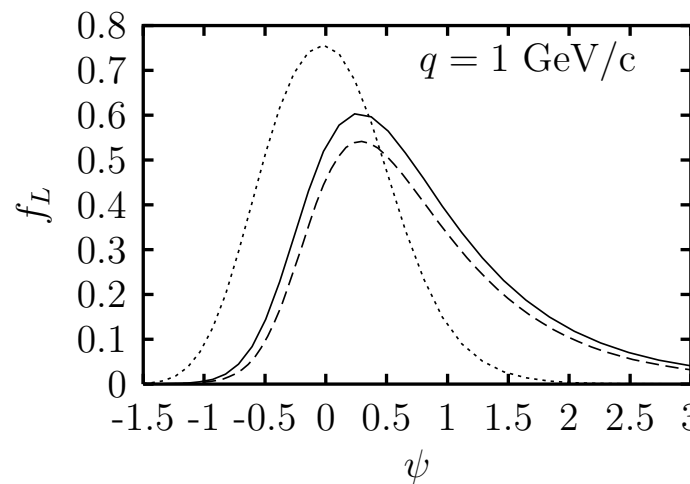
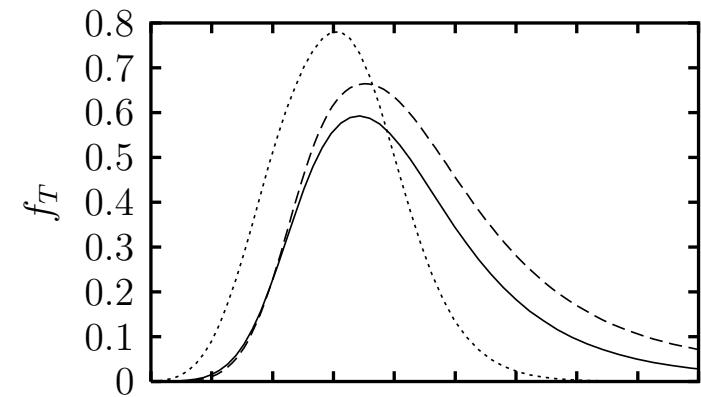
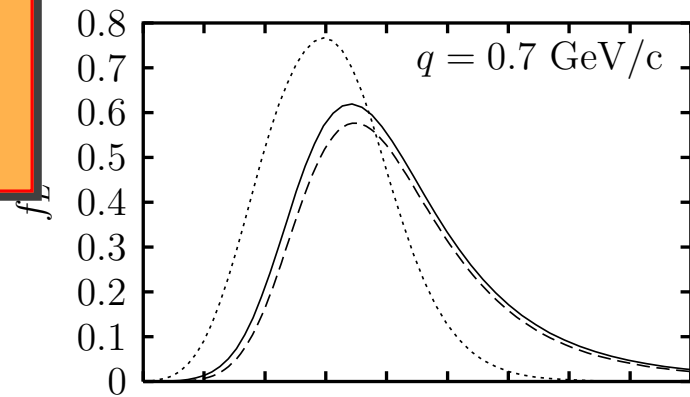
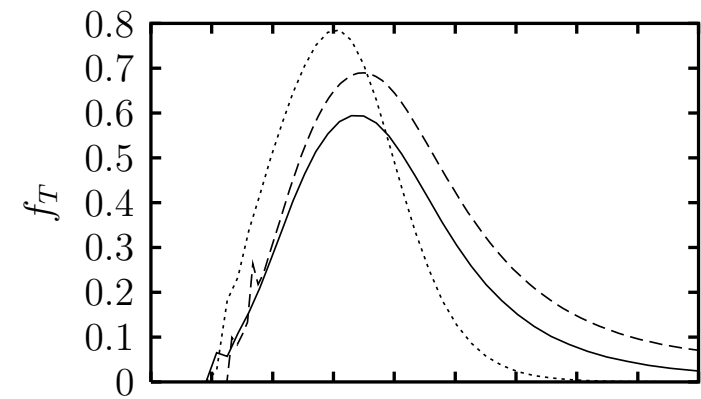
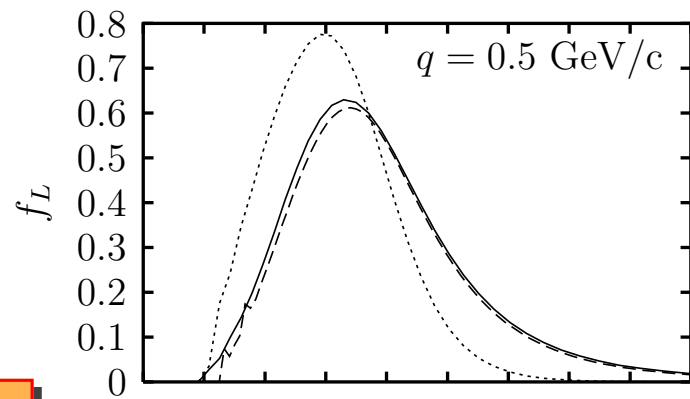
- Rewrite Dirac equation as a second-order equation for the up component $\psi_{up}(\vec{r})$
- Darwin term: $\psi_{up}(\vec{r}) = K(r, E)\phi(\vec{r})$
- The function $\phi(\vec{r})$ verifies the Schrödinger equation

$$\left[-\frac{1}{2m_N} \nabla^2 + U_{DEB}(r, E) \right] \phi(\vec{r}) = \frac{E^2 - m_N^2}{2m_N} \phi(\vec{r})$$

- Both the DEB potential $U_{DEB}(r, E)$ and Darwin term $K(r, E)$ are energy-dependent

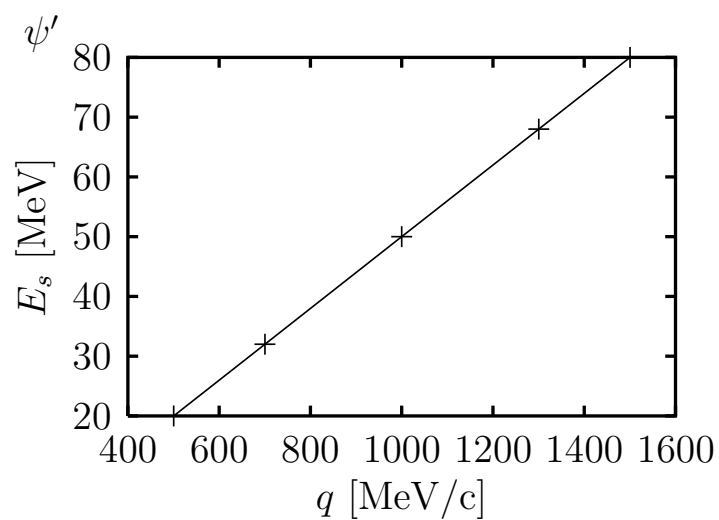
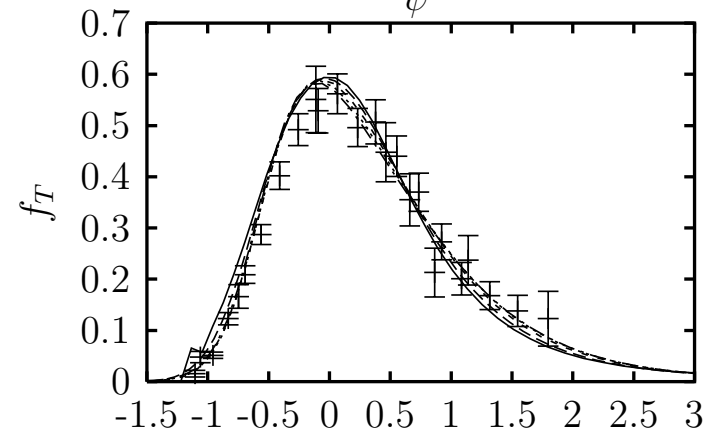
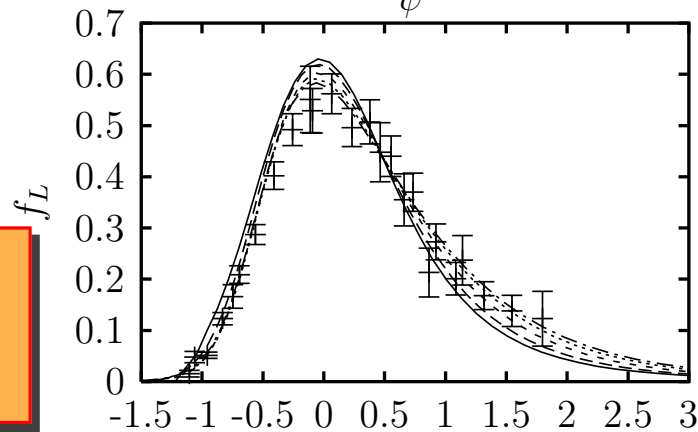
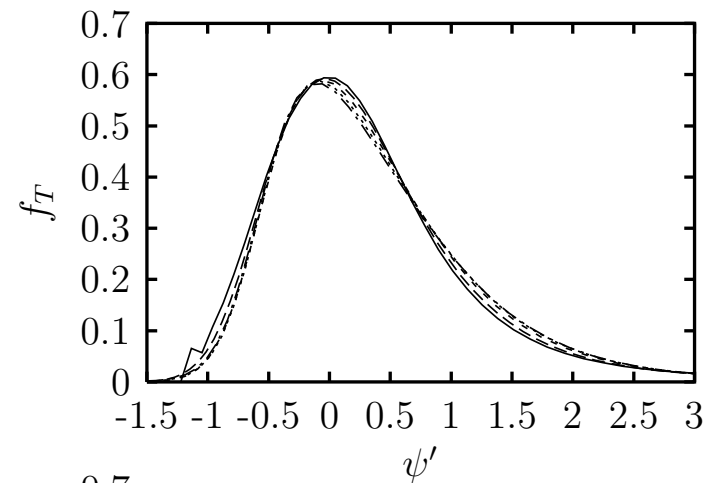
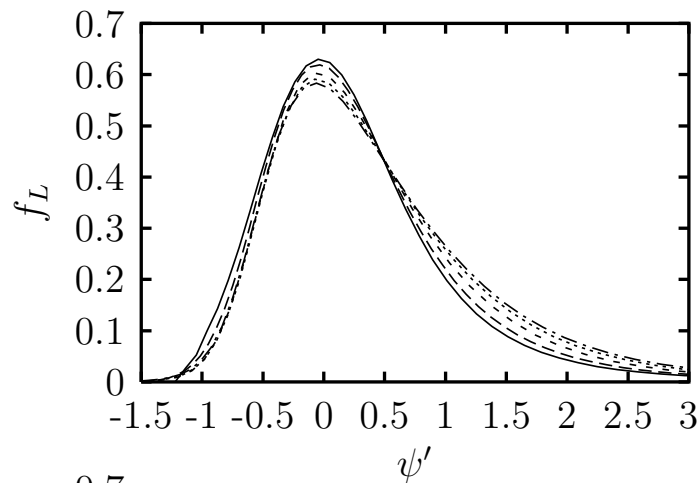
DEB+D FSI effect

Dotted: SR Woods-Saxon
Solid: SR DEB+D
Dashed: RMF

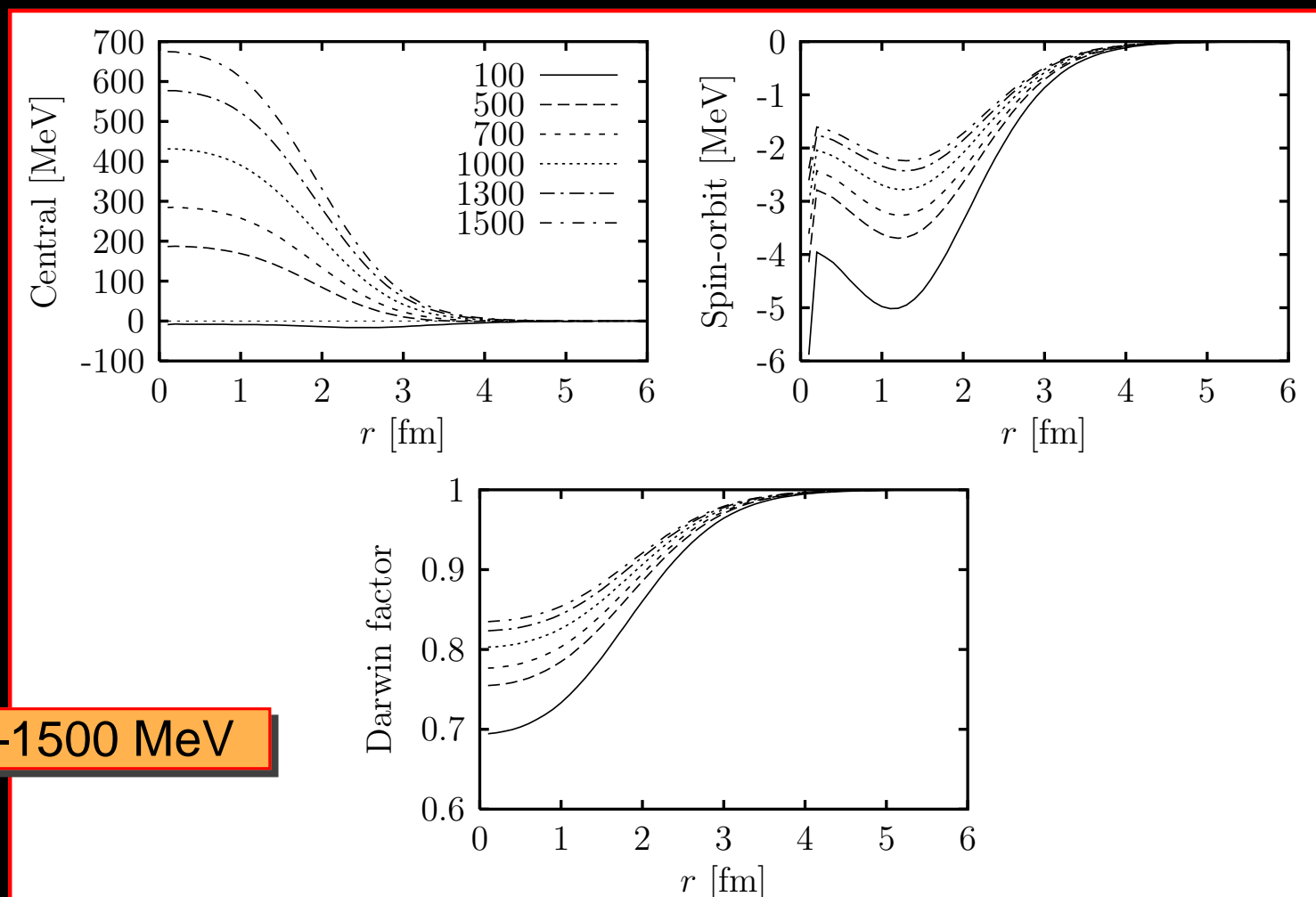


Scaling of 1st kind DEB+D

$q = 0.5, 0.7$
 $1.0, 1.3$
and $1.5 \text{ GeV}/c$



Energy dependence of DEB potential

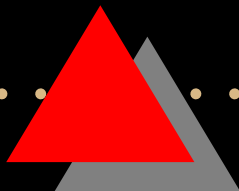
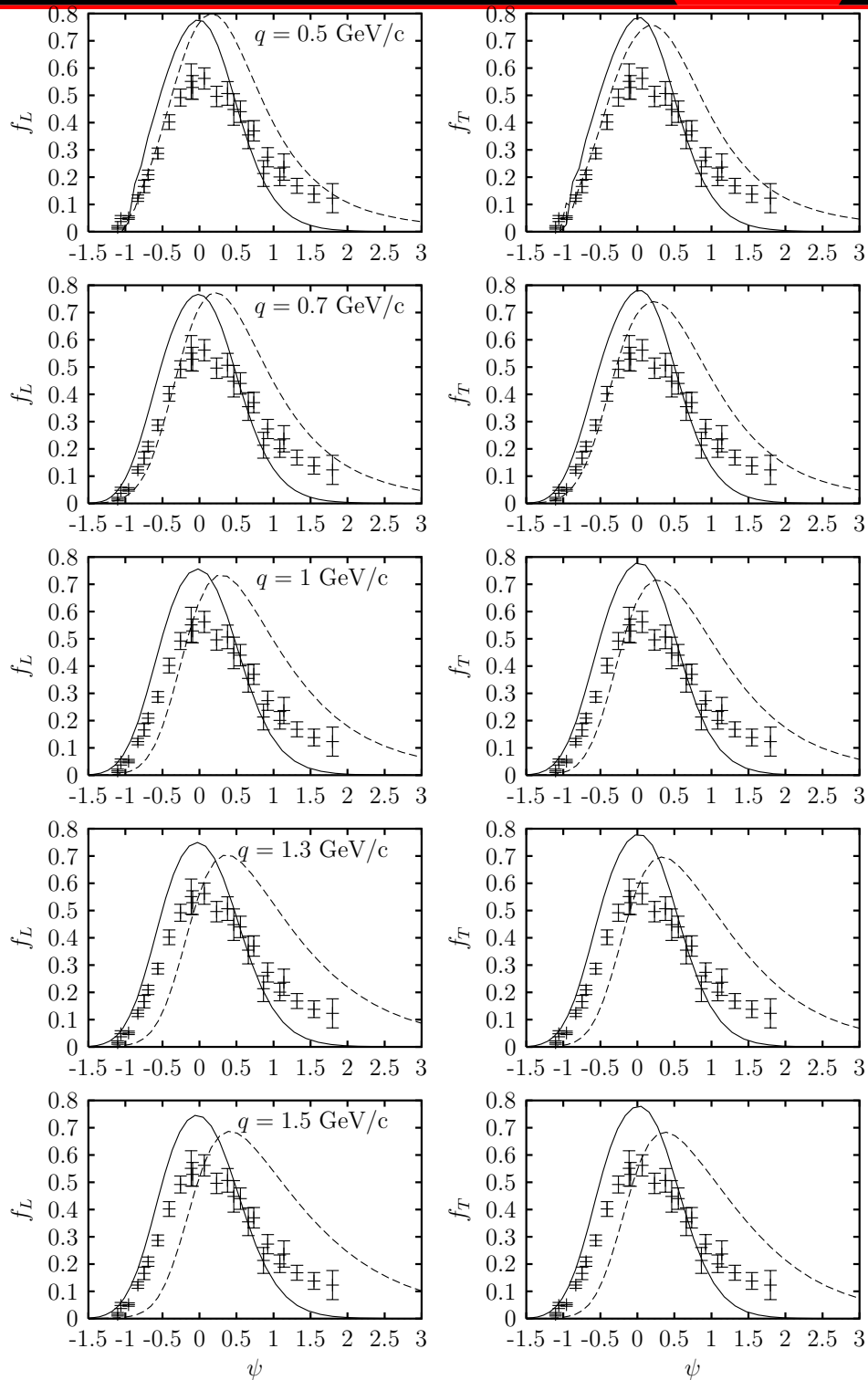


$E = 100 - 1500$ MeV



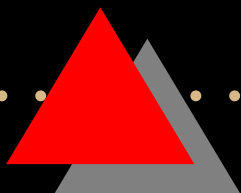
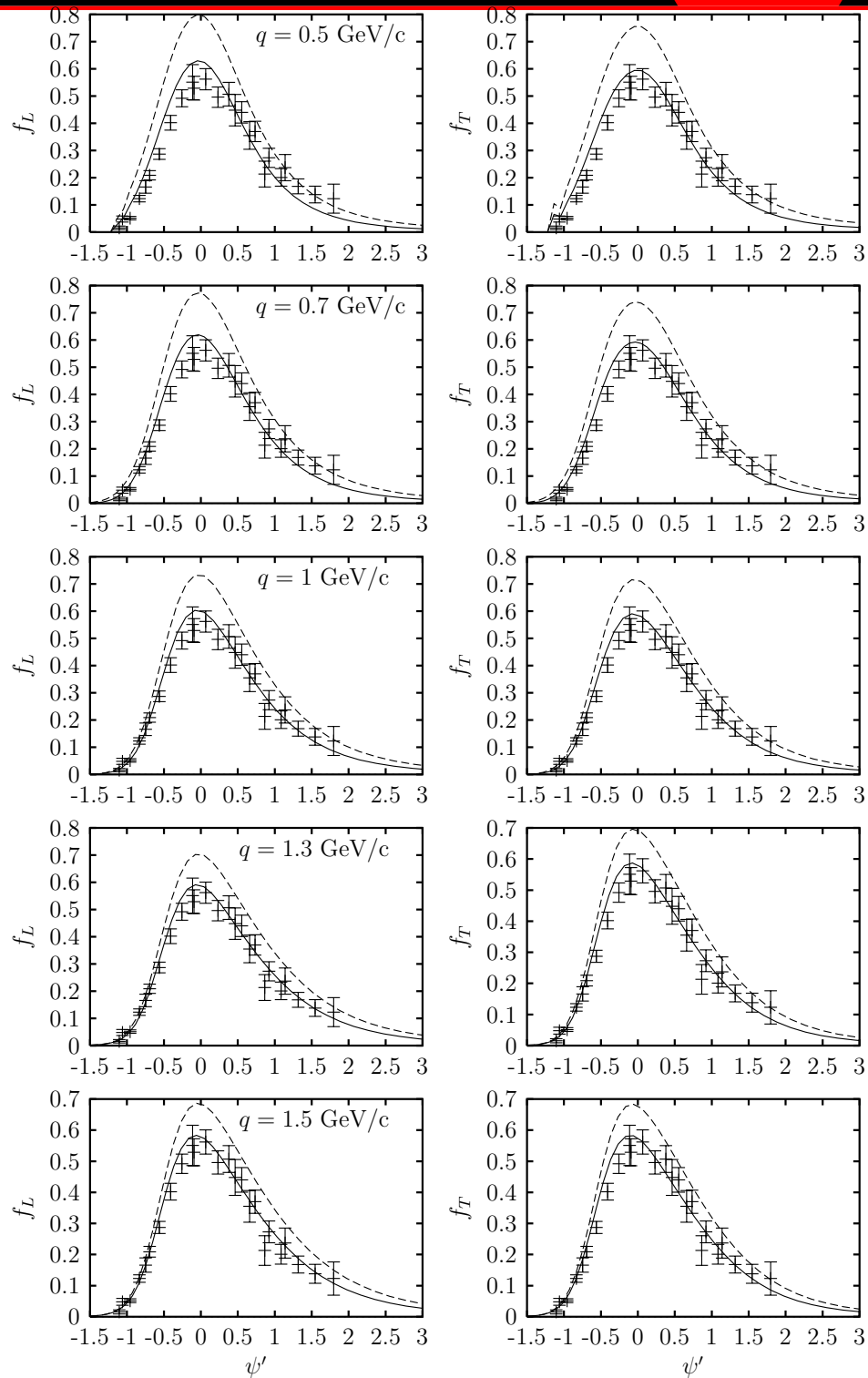
$^{12}\text{C} (e, e')$

DEB effect only
No Darwin term



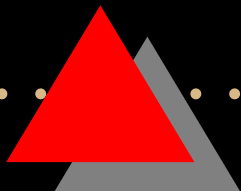
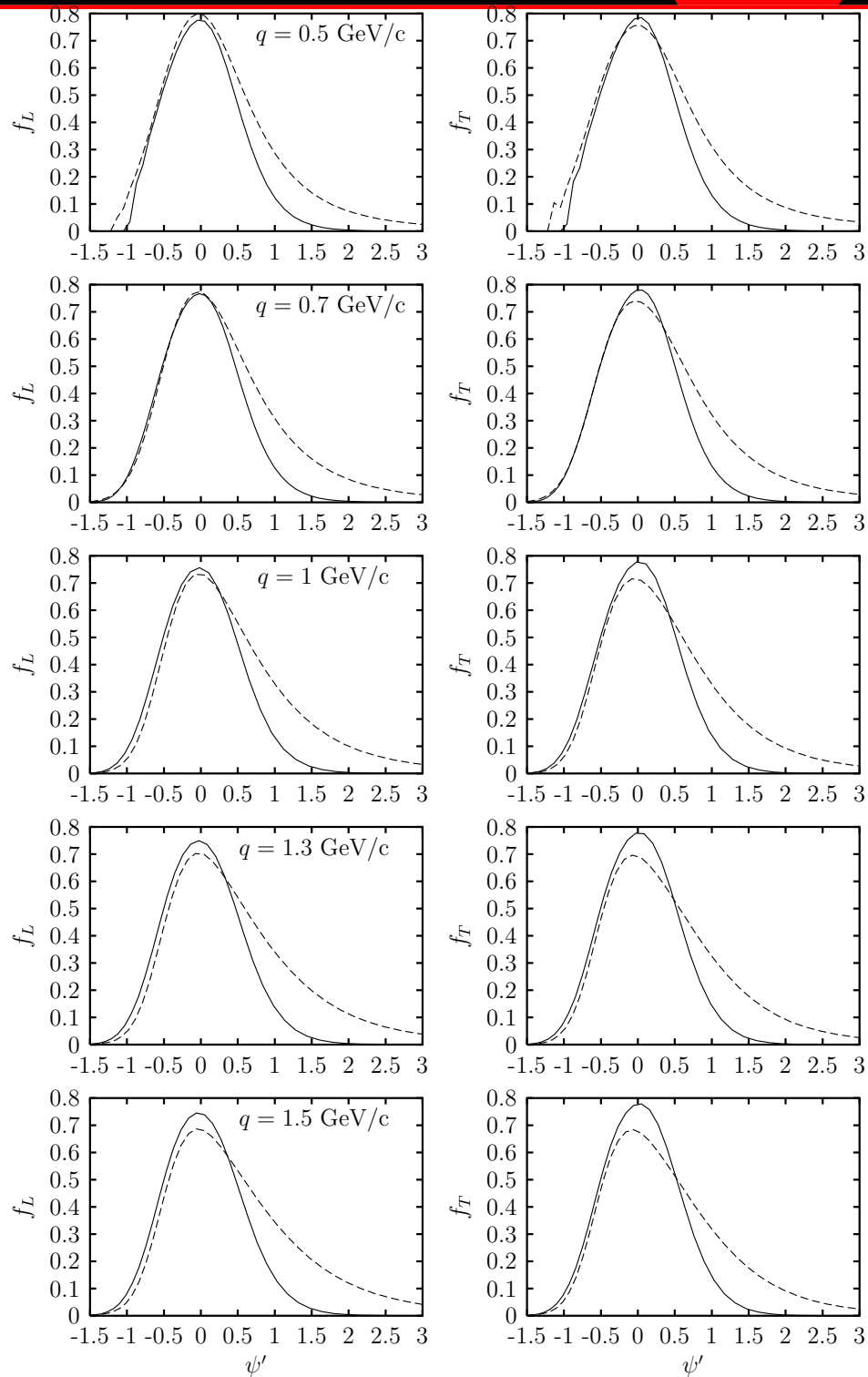
$^{12}\text{C} (e, e')$

Effect of Darwin term
With energy shift



$^{12}\text{C} (e, e')$

DEB only
with energy shift. No
darwin term



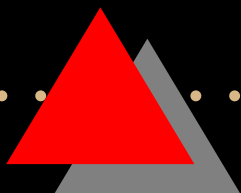
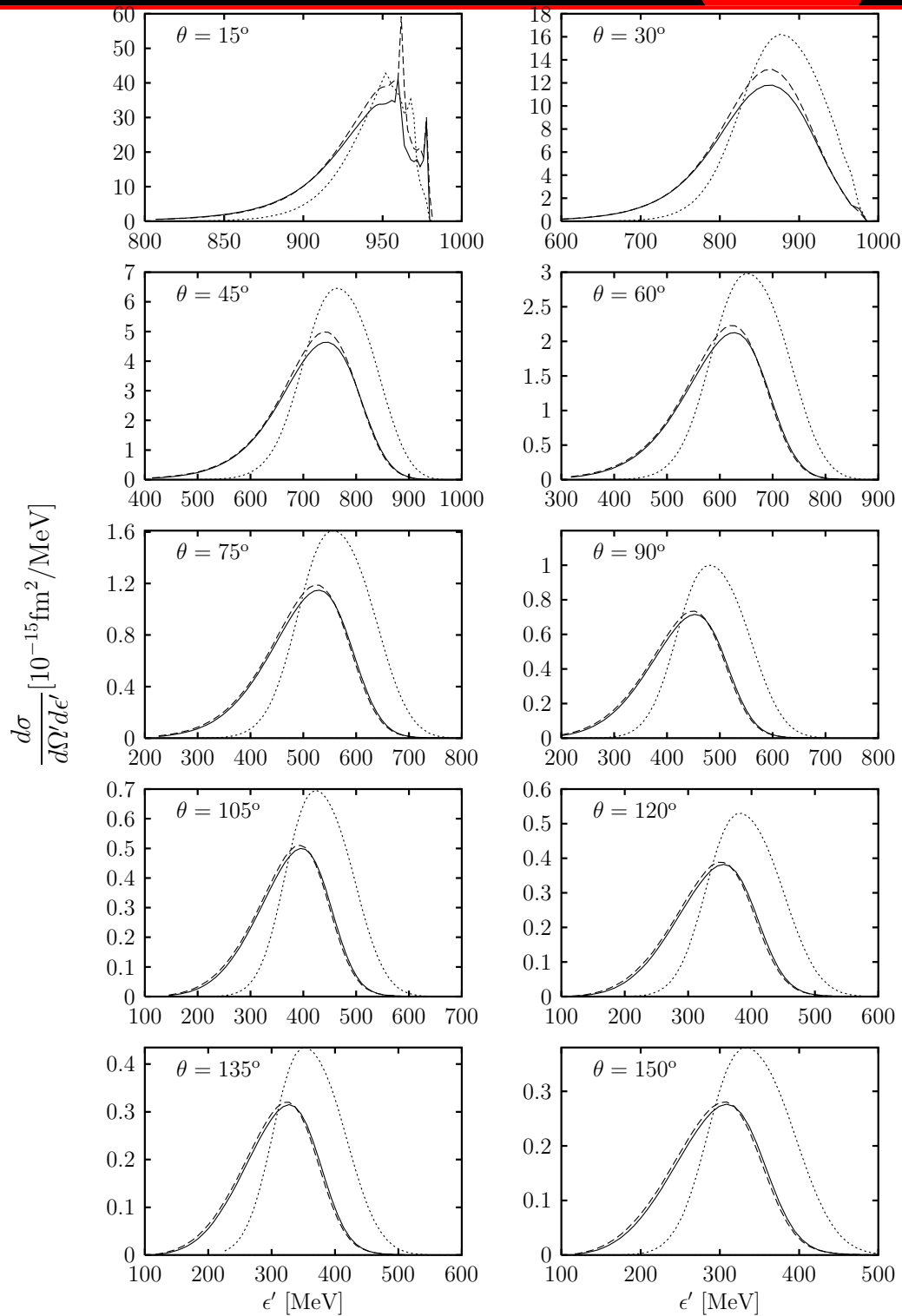
CC neutrino reactions

- SuSA reconstruction of the (ν_μ, μ^-) cross section from the (e, e') one
- Test of the SuSA in the CSM
- The CSM electromagnetic scaling function is used to compute neutrino cross sections.
- Compare with the exact CSM result

$^{12}\text{C}(\nu_{\mu}, \mu^{-})$

$\epsilon = 1 \text{ GeV}$

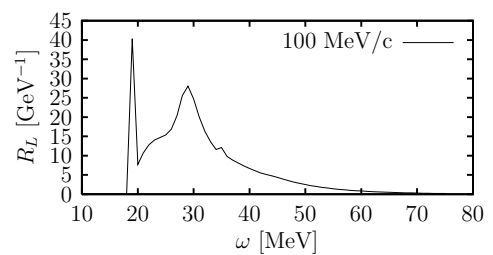
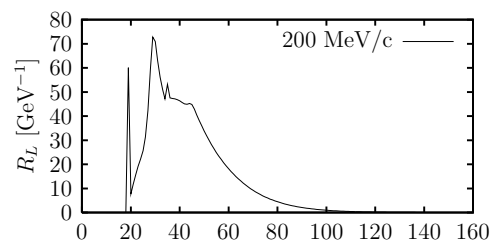
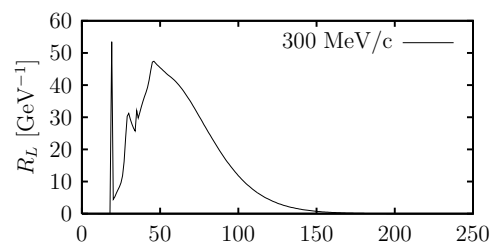
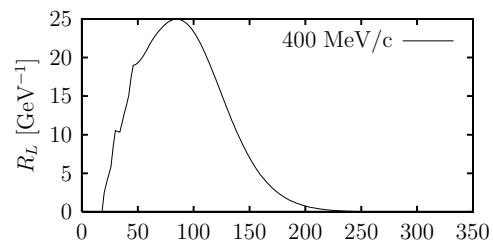
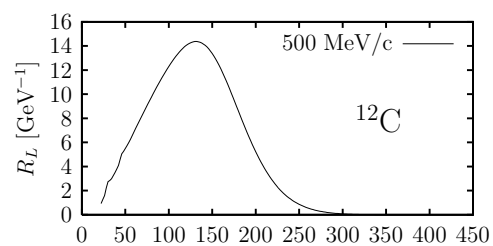
Dotted: Woods-Saxon
Solid: DEB+D
Dashed: SuSA



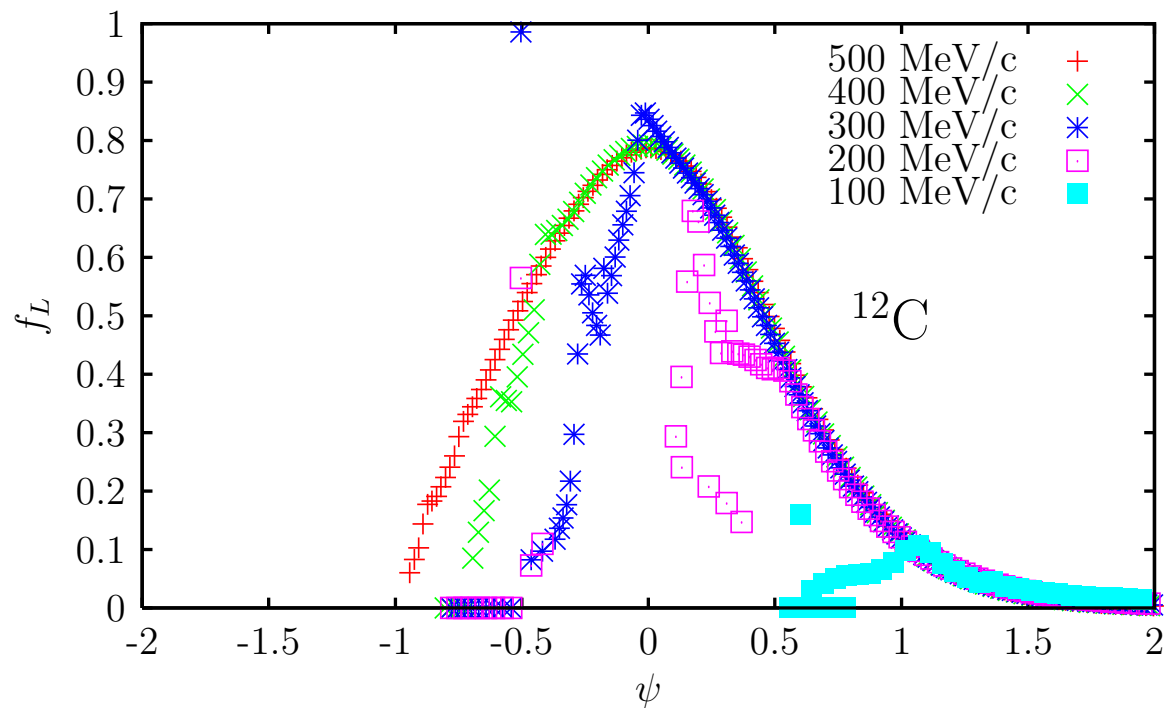
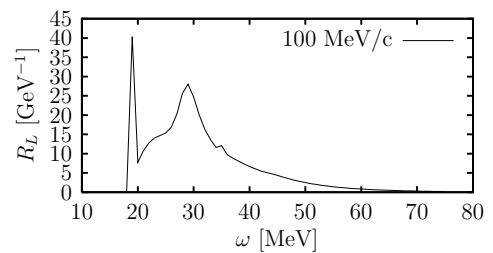
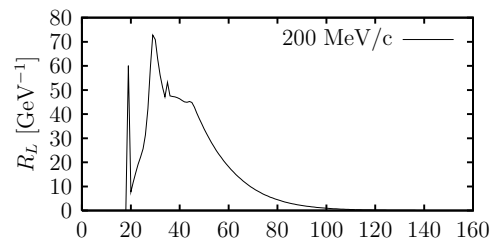
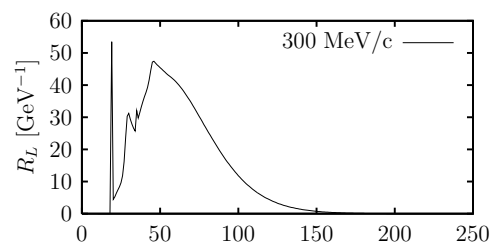
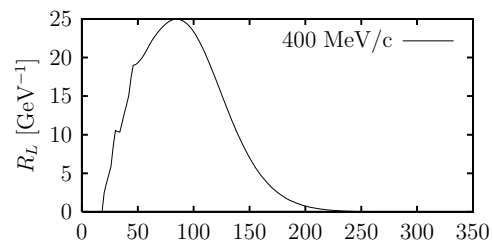
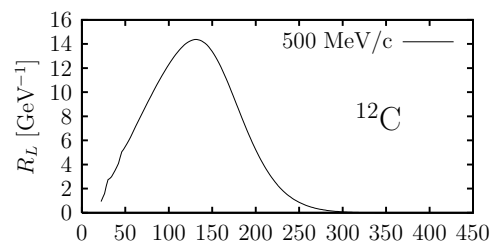
Scaling violation for low q



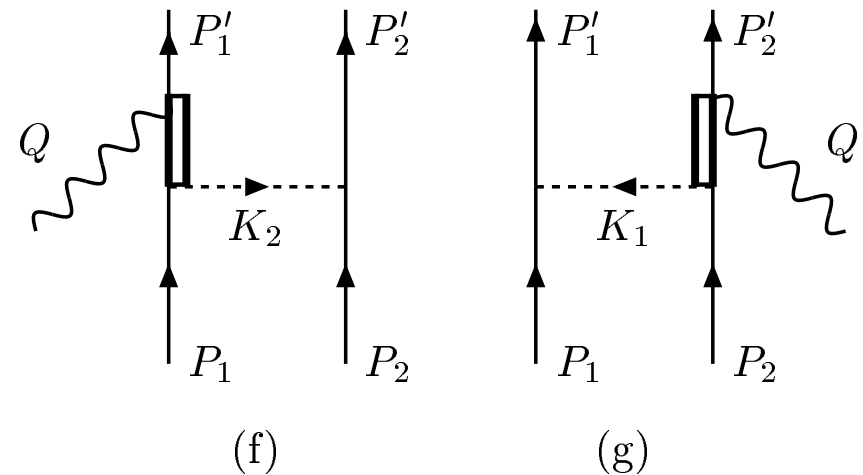
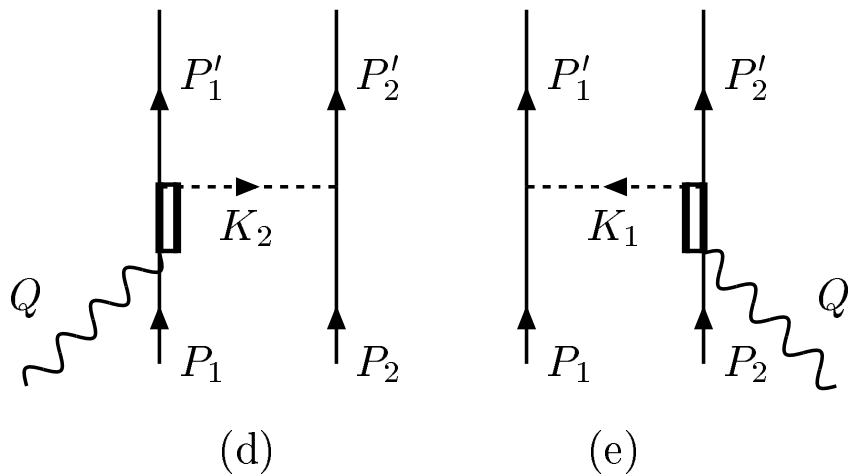
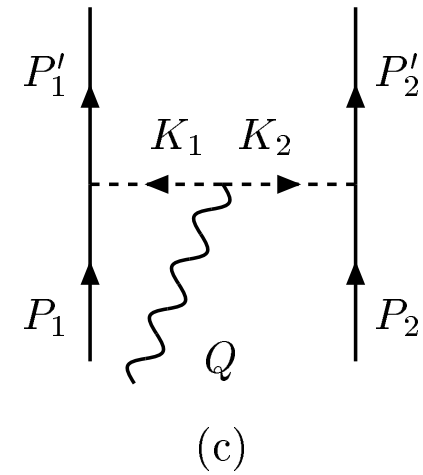
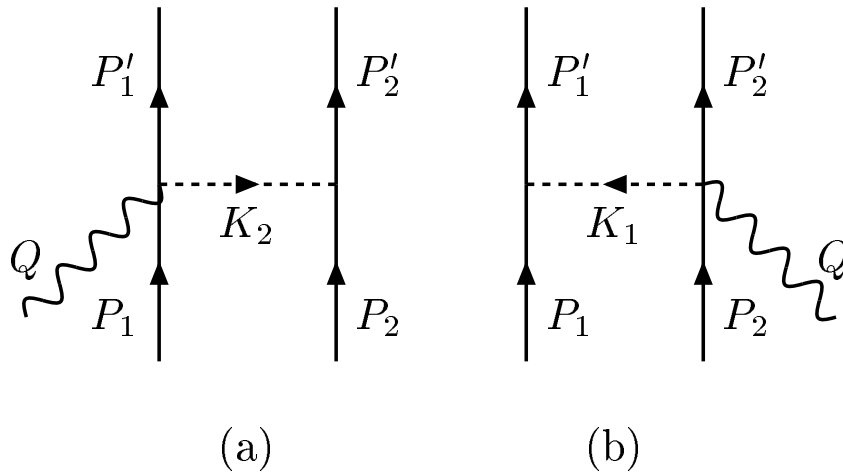
Scaling violation for low q



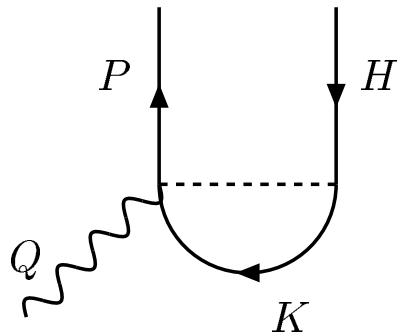
Scaling violation for low q



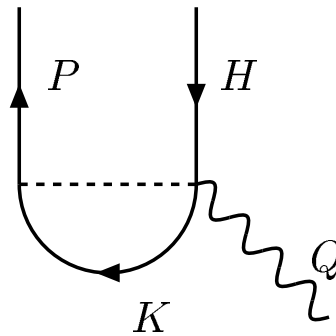
4 Meson-Exchange Currents



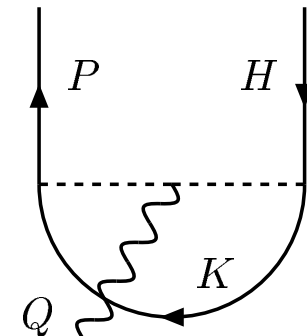
1p-1h matrix elements



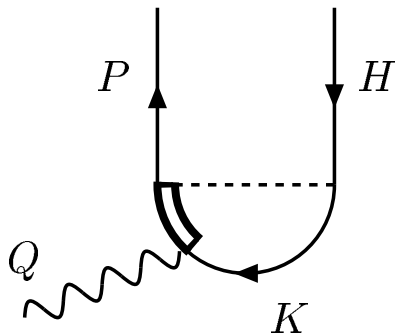
(a)



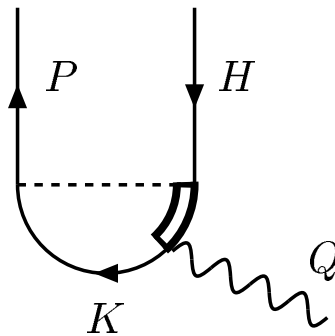
(b)



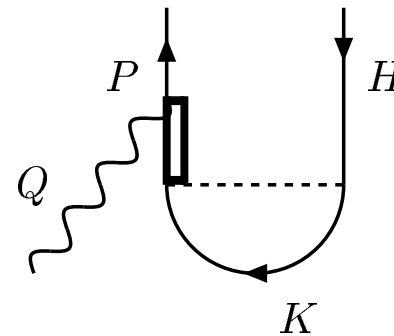
(c)



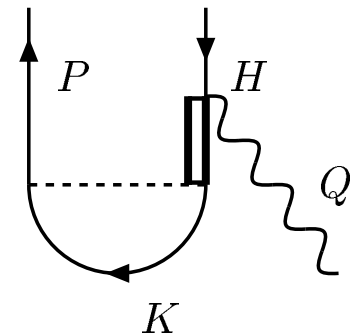
(d)



(e)



(f)



(g)

MEC Semi-relativistic expansion

$$\vec{J}_{\Delta} = \frac{i}{\sqrt{1+\tau}} \frac{2}{9} \frac{G_1}{2m_N} \frac{f_{\pi N \Delta} f}{m_{\pi}^2} \frac{1}{m_{\Delta} - m_N} \frac{\vec{k}_2 \cdot \vec{\sigma}^{(2)}}{m_{\pi}^2 - K_2^2} \cdot \left\{ 4\tau_3^{(2)} \vec{k}_2 - [\vec{\tau}^{(1)} \times \vec{\tau}^{(2)}]_z \vec{\sigma}^{(1)} \times \vec{k}_2 \right\} \times \vec{q} + (1 \leftrightarrow 2)$$

$$\vec{J}_{Seagull} = -\frac{i}{\sqrt{1+\tau}} \frac{f^2}{m_{\pi}^2} F_1^V \frac{\vec{k}_2 \cdot \vec{\sigma}^{(2)}}{m_{\pi}^2 - K_2^2} \times [\vec{\tau}^{(1)} \times \vec{\tau}^{(2)}]_z \vec{\sigma}^{(1)} + (1 \leftrightarrow 2)$$

Test of the SR MEC RFG vs SRFG (static propagator) $^{12}\text{C}(e, e')$

Transverse response
 Δ -OB interference

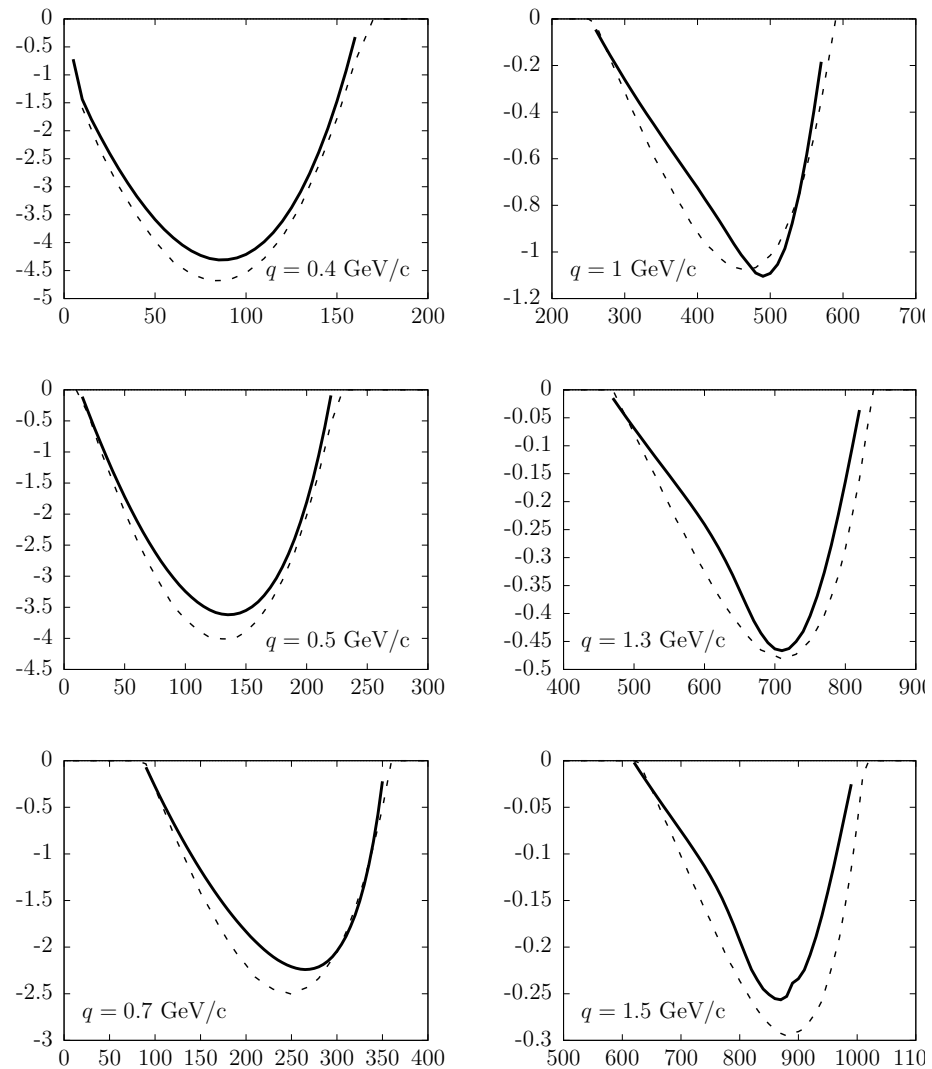
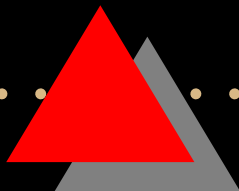
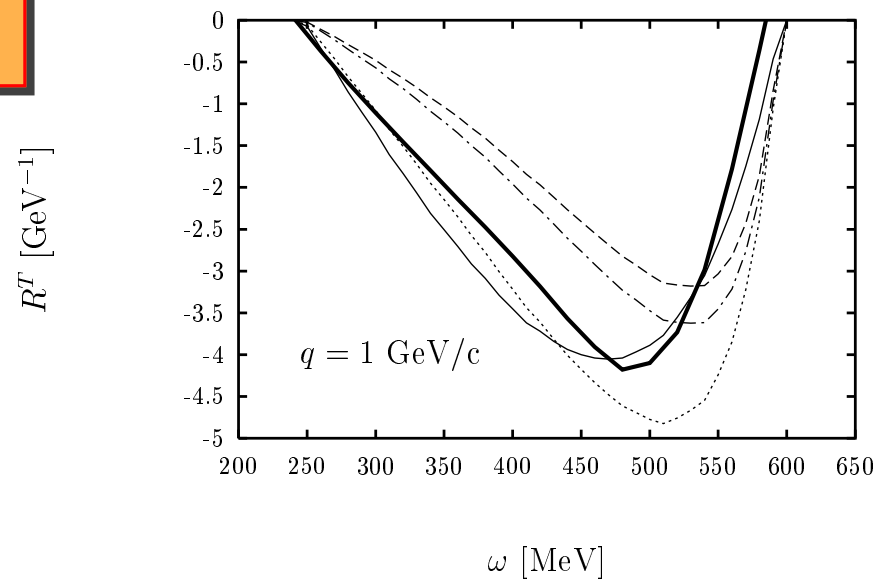
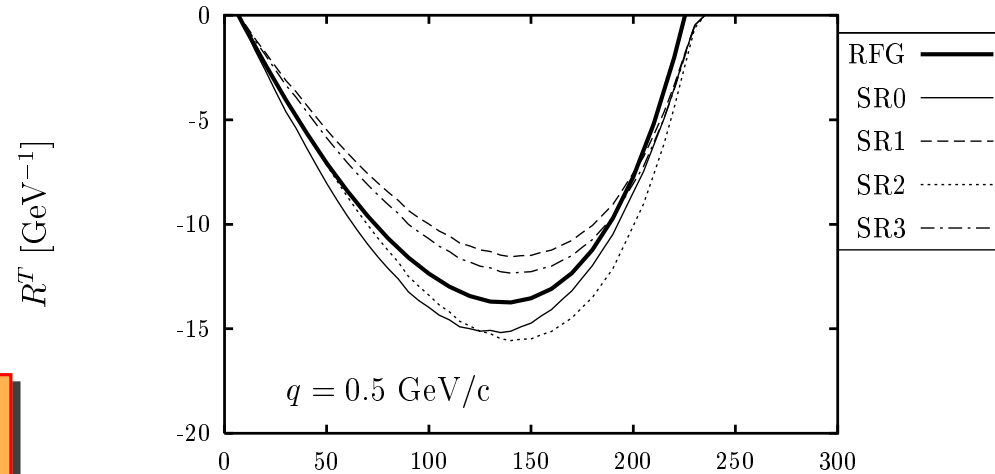


Fig.1. Interference T response of OB and Δ current. Solid lines: RFG. Dashed lines: SRFG with static Δ propagator and static pion propagator.



Semi-relativistic expansion of MEC

dynamical Δ propagator effect
From Amaro et al.,
PRC 68, 014604 (2003)

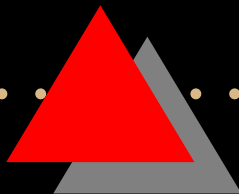
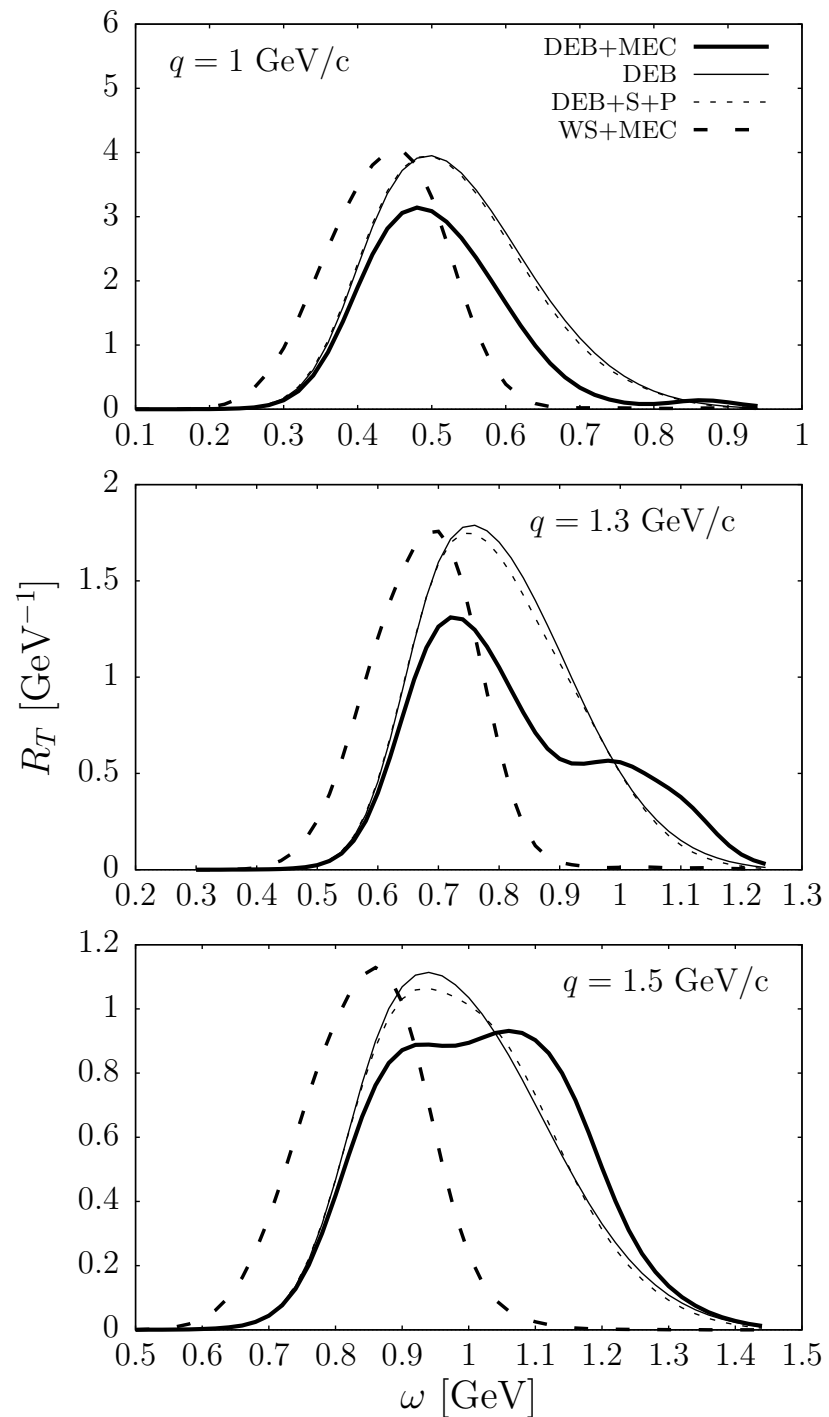


The MEC bump

Total MEC + DEB results

$^{12}\text{C}(e, e')$

Transverse response



Woods-Saxon results $^{12}\text{C}(e, e')$ No MEC bump

Transverse response

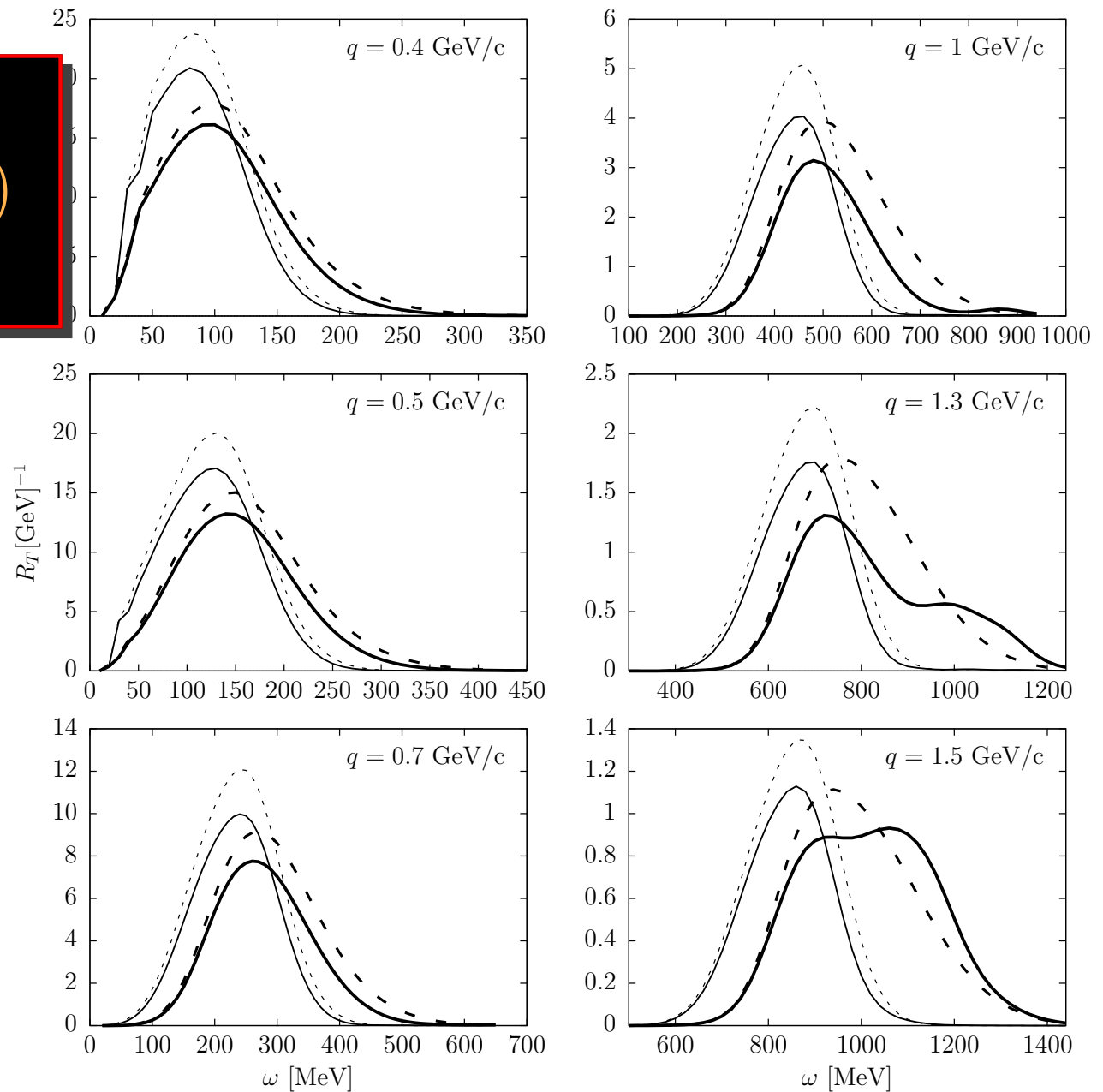
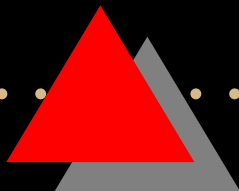
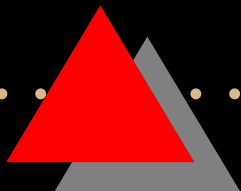
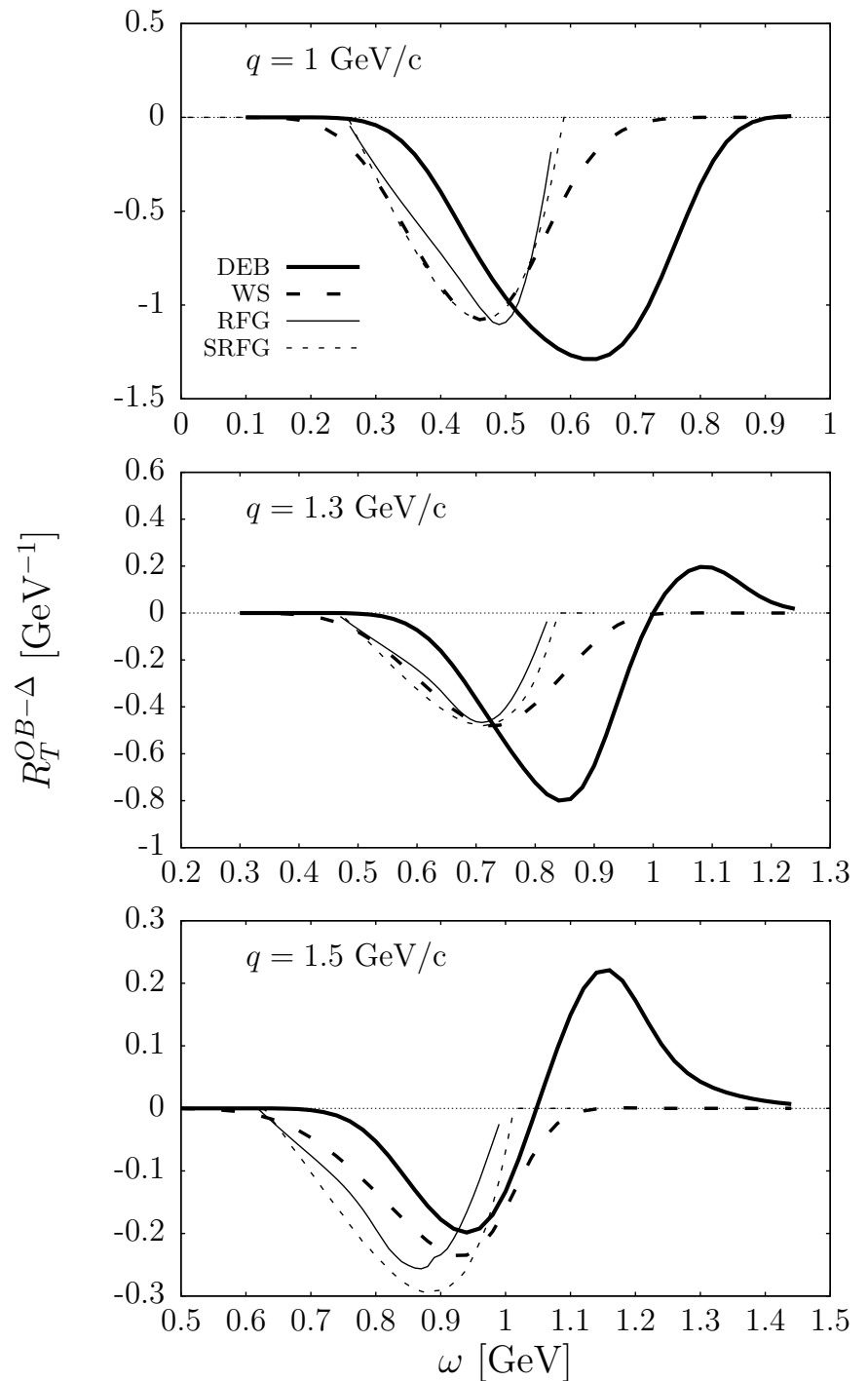


Fig.5. T response with MEC (solid) and without MEC (dashed).
Thick lines: DEB potential. Thin lines: WS potential.



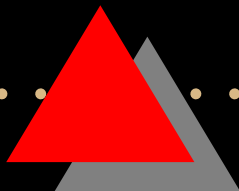
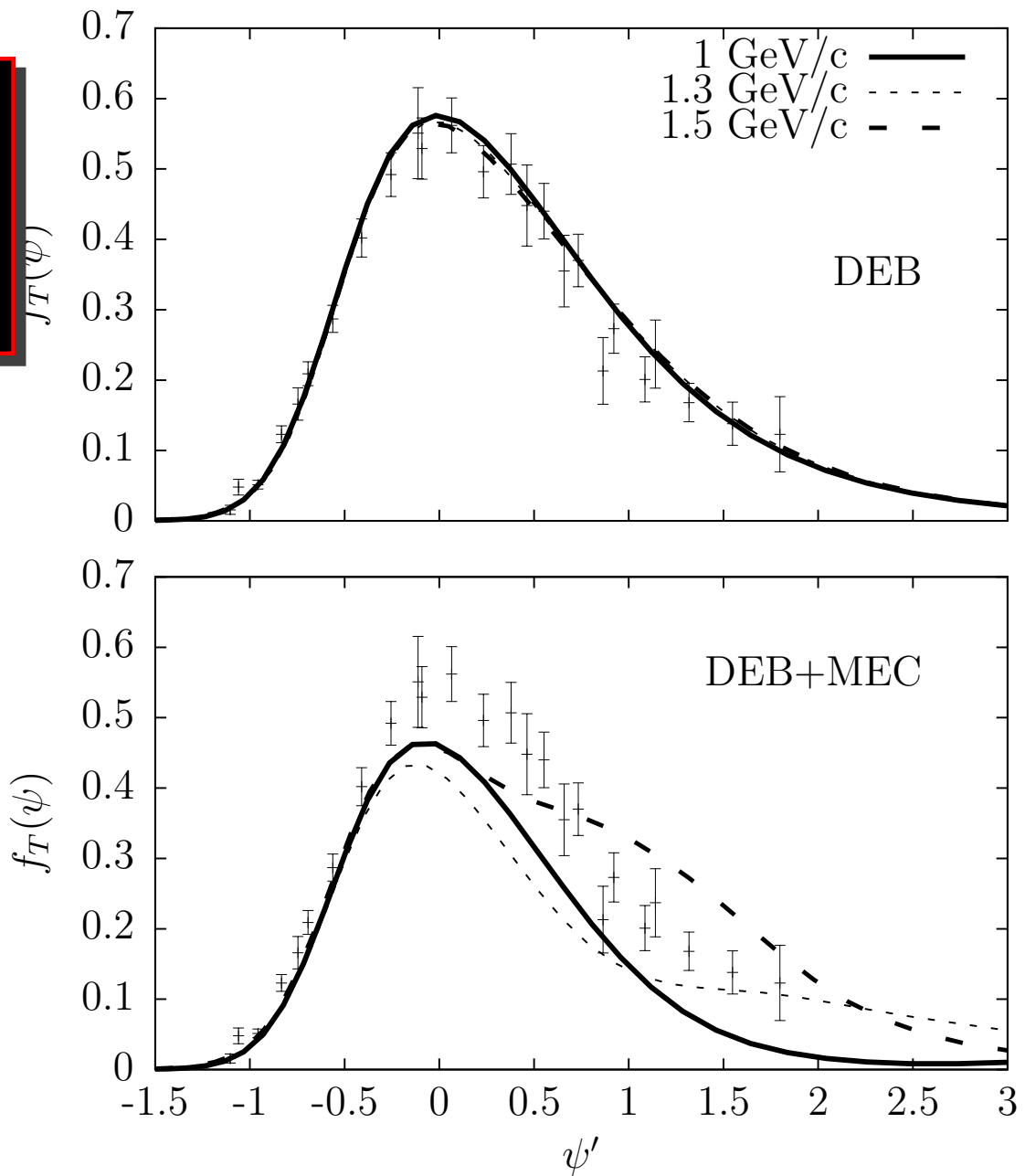
MEC+DEB compared with Woods-Saxon RFG and SRFG $^{12}\text{C}(e, e')$

Δ -OB interference
Transverse response
Change of sign
for $\omega > 1$ GeV



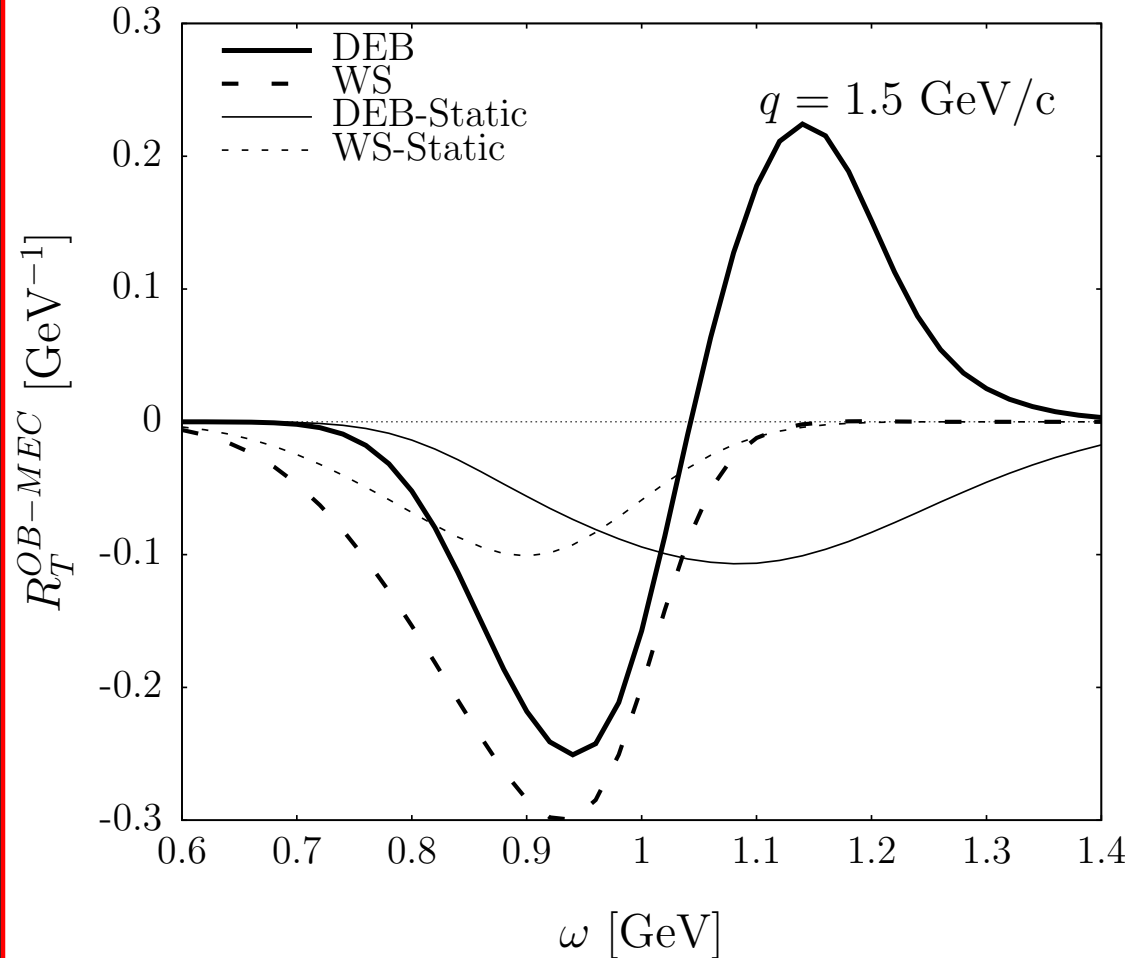
MEC+DEB scaling breaking $^{12}\text{C}(e, e')$

Transverse
scaling function



MEC effect - Static pion propagator

WS and DEB
 Static and dynamical
 pion propagator
 Transverse response
 $^{12}\text{C}(e, e')$



MEC+DEB, static and dynamical pion propagator results vs RFG and SRFG

$^{12}\text{C}(e, e')$

OB- Δ interference
Transverse response

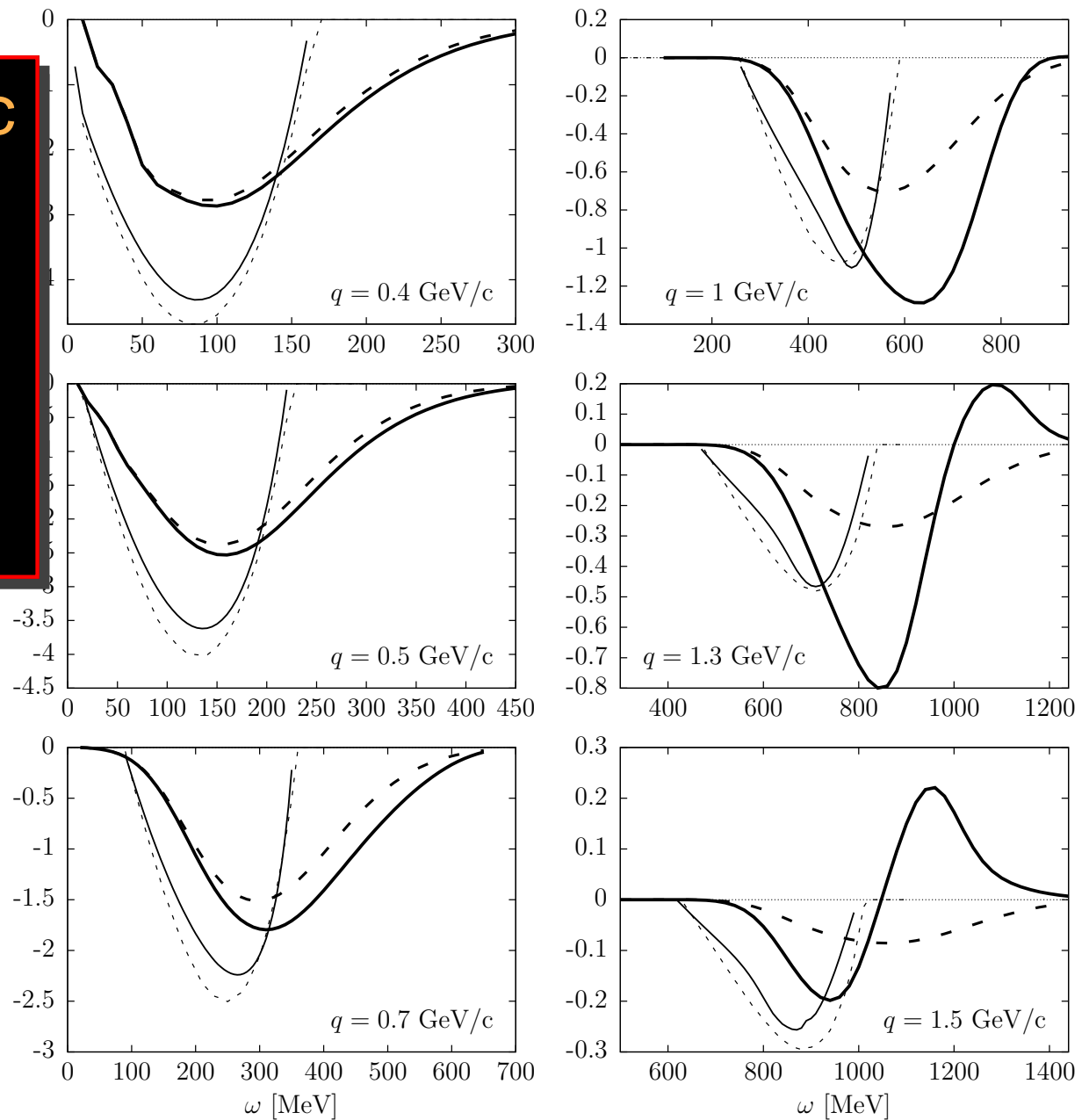
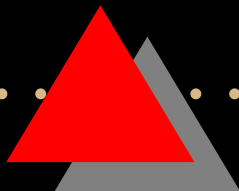


Fig.3. Interference T response of OB and Δ current. Thick solid lines: DEB with dynamic pion propagator. Thick dashed lines: DEB with static pion propagator. Thin Dashed lines: SRFG with static Δ propagator and static pion propagator. Thin solid lines: RFG



WS static and dynamical pion propagator results vs RFG and SRFG $^{12}\text{C}(e, e')$

OB- Δ interference
Transverse response

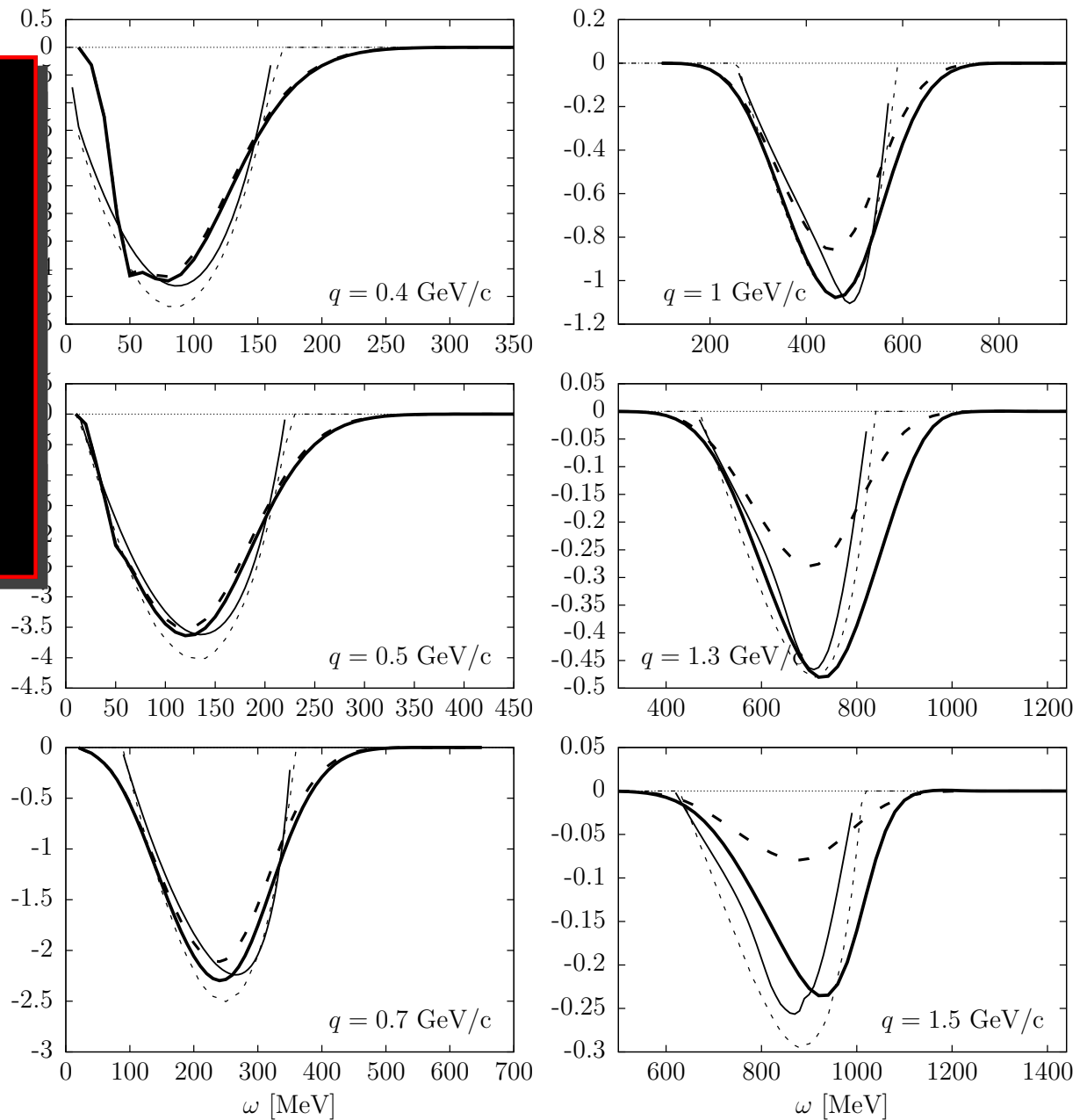
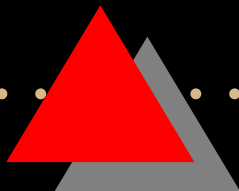


Fig.4. Interference T response of OB and Δ current. Thick solid lines: WS with dynamic pion propagator. Thick dashed lines: WS with static pion propagator. Thin Dashed lines: SRFG with static Δ propagator and static pion propagator. Thin solid lines: RFG



WS static and dynamical pion propagator vs forward diagram contribution only
 $^{12}\text{C}(e, e')$

OB- Δ interference
 Transverse response

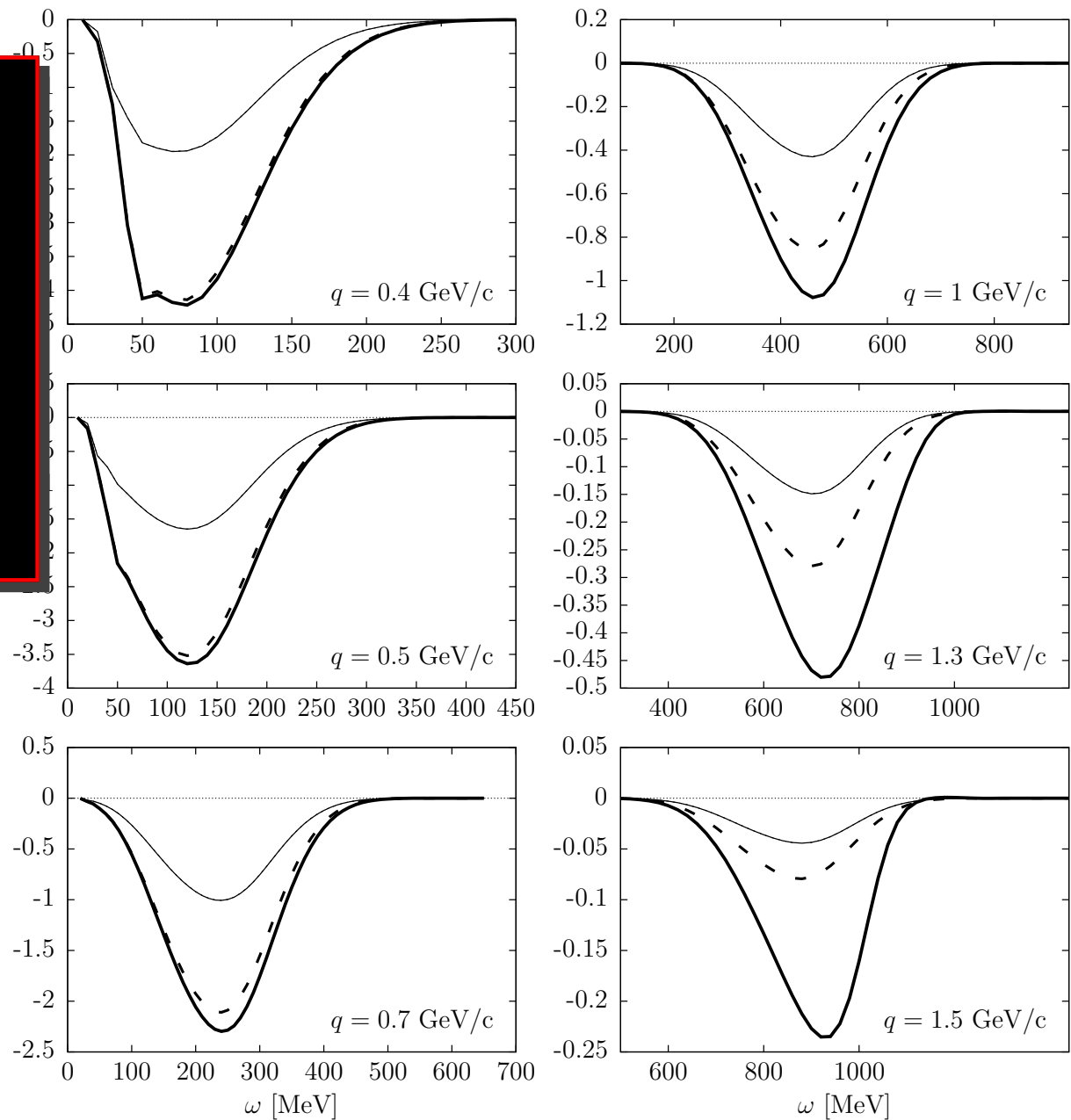
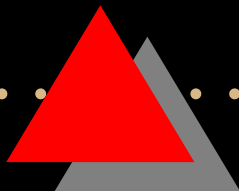


Fig.6. Interference T response of OB and Δ current. Thick solid lines: WS with dynamic pion propagator. Thick dashed lines: WS with static pion propagator. Thin lines: WS with forward diagrams contribution only (there is no difference between dynamic or static pion propagator)



DEB static and dynamical pion propagator vs forward diagram contribution only

$^{12}\text{C}(e, e')$

OB- Δ interference
Transverse response

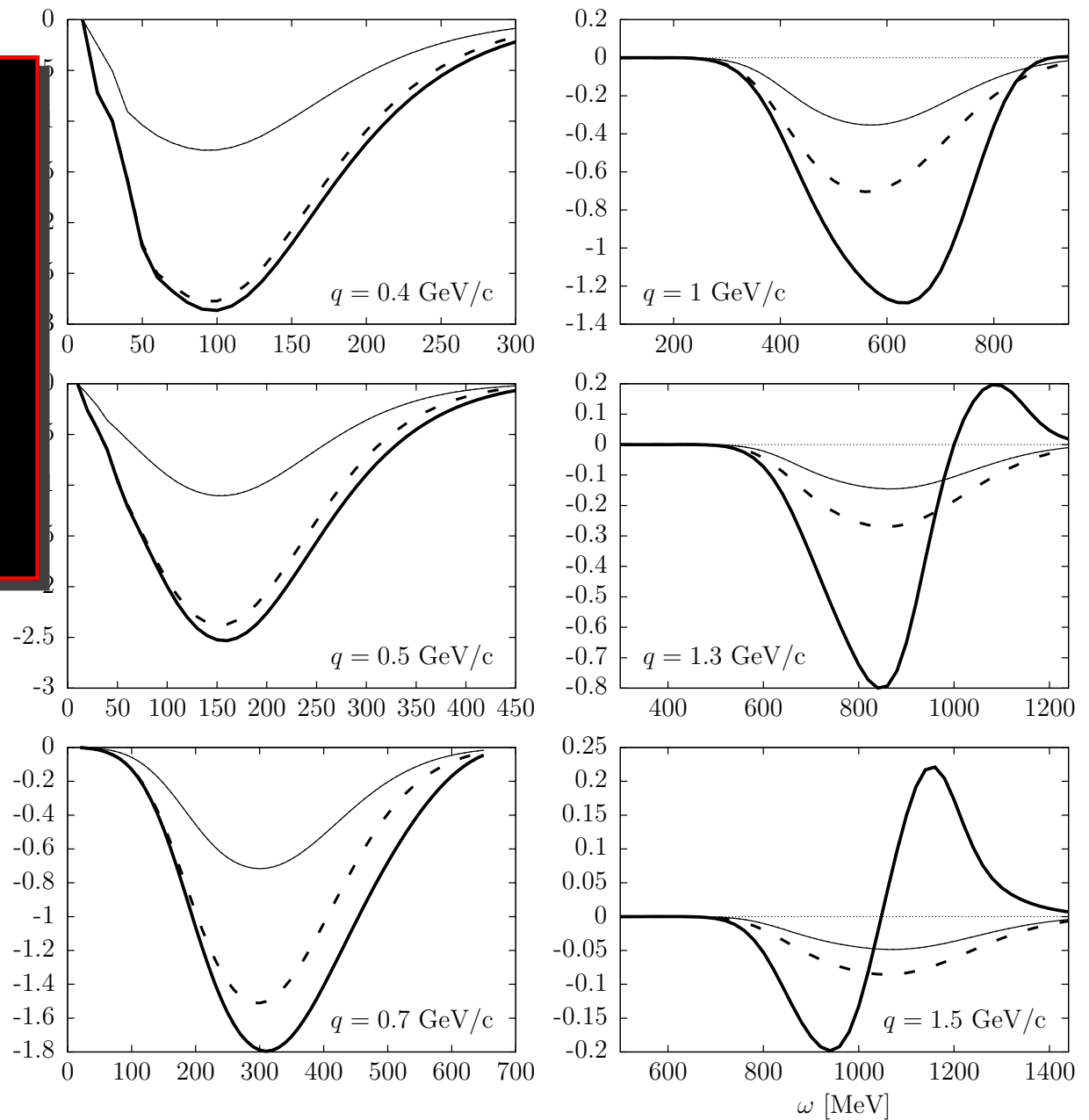
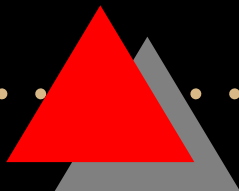


Fig.7. Interference T response of OB and Δ current. Thick solid lines: DEB with dynamic pion propagator. Thick dashed lines: DEB with static pion propagator. Thin lines: DEB with forward diagrams contribution only (there is no difference between dynamic or static pion propagator)



Conclusions:

Semi-relativistic shell model

- Incorporate relativistic effects in existing models
- Applications to intermediate energies
- Study of the scaling properties of electromagnetic responses. The model verifies superscaling.
- The DEB+D model of FSI reproduces the experimental scaling function
- It is possible to reconstruct via SuSA the (ν_μ, μ^-) cross section from the (e, e') one for $q > 500$ MeV/c
- The SR shell model can be used to evaluate the MEC contribution for high energy (hard to compute in exact relativistic models)

Conclusions: MEC

- The MEC give an important contribution in the high energy tail of the 1p-1h transverse response
- The MEC bump is due to a change of sign of the MEC contribution for energy transfer $\omega > 1$ GeV
- The change of sign is produced by the dynamical pion propagator
- The MEC bump is only predicted when the FSI produce a dynamical enhancement of the high-energy tail (DEB potential)
- The MEC contribute to the scaling violations for $\psi > 0$ for $q > 1$ GeV/c

THE END

